Paper VII

Application of water vapor sorption measurement for porosity characterization of hardened cement pastes

M. Wu, B. Johannesson, M. Geiker

Accepted by: *Construction and Building Materials, 2014*

Application of water vapor sorption measurement for porosity characterization of hardened cement pastes

Min Wu[a], Björn Johannesson[a], and Mette Geiker[b]

a. Department of Civil Engineering, Building 118, Technical University of Denmark, 2800 Lyngby, Denmark

b. Department of Structural Engineering, Norwegian University of Science and Technology, Trondheim, Norway

Abstract

Water vapor sorption can be used to study important properties of porous materials including specific surface area and pore size distribution (PSD). However, the data analysis is somewhat inconsistent in literature. In this work, the important factors influencing the analyzed results using sorption data were reviewed. Water vapor sorption measurements were then applied to two hardened cement pastes and one model porous material MCM-41. The specific surface area was calculated based on different equations accounting for multilayer adsorption and the PSD was analyzed from both the absorption and the desorption isotherms for comparison. The calculated specific surface area was quite dependent on which equation is considered for multilayer adsorption. For the studied hardened cement pastes, three characteristic peaks were found in the calculated PSD curves from the desorption isotherms with corresponding radii of 1.4, 1.8 and 3.0 nm while the peak at 1.4 nm was missing in the PSD curves calculated from the absorption isotherm. The network theory, suggesting desorption is controlled by the pore entry sizes while absorption is controlled by the interior pore sizes, tends to be of great relevance in explaining the results.

Keywords: Microstructure, specific surface area; pore size distribution; adsorption; cement paste; network theory.

1. Introduction

Porosity is one of the most important characteristics of cement based materials. Vapor sorption measurement has been widely used to determine the specific surface area and the pore size distribution of porous materials [1, 2]. The calculation of specific surface area is normally based on the classical BET theory [3]. With respect to the pore size distribution, the method proposed by Barret, Joyner and Halenda (the BJH model) [4] is widely adopted. The BJH model is based on the assumption that there are two types of liquid existing simultaneously in the pores of a material due to different binding mechanisms, i.e., adsorption and capillary condensation. This assumption allows the determination of the pore size distribution for pores in the meso-size and micro-size range (following the classification of International Union of Pure and Applied Chemistry (IUPAC) [2]). For clarification purpose, a note is made here about the terminology "adsorption" and "absorption". In many cases, e.g., see [2], "adsorption" is used in describing the process of the liquid uptake, including both the adsorbed and the capillary condensed liquid. Other authors, e.g., see [5, 6], use "absorption" to describe exactly the same content, i.e., including both types of liquid uptake. Since the BJH model will be used throughout this study and to avoid any confusion, the expression "absorption" will be used to describe the combined

effect of both multilayer adsorption and capillary condensation while "adsorption" simply refers to the liquid fixed due to multilayer adsorption.

Sorption measurement using nitrogen is perhaps the most common technique adopted in the context of porosity characterization and it has been studied rather extensively, e.g., see [1, 7, 8]. However, a comparison study performed by Hagymassy et al. [9] using both nitrogen and water vapor in characterizing hardened cement paste samples has demonstrated that both the total calculated pore volume and the calculated surface area using water vapor data are much larger compared with that using nitrogen data. The main reason was explained by the fact that the nitrogen cannot penetrate into the entire pore system of hardened cement pastes due to the relatively big molecular size. It was, further, pointed out by the same authors that the use of nitrogen will result in that not only the smallest pores but also many big pores, which are the so-called ink-bottle pores with small entry or neck sizes but big interior sizes, are left out of consideration in the measurement using nitrogen. That is the smallest pore entries or necks constraint the penetration of nitrogen molecules into the body of ink-bottle pores. Consequently, the pore structure analysis using nitrogen was concluded to be of little value in studying the porous materials of complex pore structure with wide distribution of pore sizes, e.g., the hardened cement pastes. As the main purpose of this work is to study hardened cement pastes, water vapor is considered more suitable than nitrogen in the context of the porosity characterization. Another reason for using water vapor in studying cement based materials is that the pre-drying of the samples can be avoided compared with that using nitrogen since the drying process in some cases results in certain alteration of the pore structure of hardened cement pastes [10].

Sorption behavior of water vapor on porous materials can be used to study important characteristics of the materials, e.g., the specific surface area and the pore size distribution. As an indirect method, some important factors which influence the analyzed results using sorption data need to be considered.

1.1. Equations accounting for multilayer adsorption

The calculation of the specific surface area is based on the equation considered for multilayer adsorption. A number of equations have been developed and the most representative ones are discussed as follows. It should be noted that the calculated specific surface area of a material for most cases would be different if different equations accounting for multilayer adsorption are considered.

The first sound theoretical development of the relation between the amount of adsorbed vapor and the relative pressure under equilibrium is attributed to Langmuir [11]. However, the limitation of the Langmuir model is that adsorption is restricted to the monolayer. A major step in the understanding of adsorption is the development of the BET multilayer adsorption theory Brunauer et al. [3]. After the development of the BET theory, a number of adsorption equations have been developed using the similar concepts. A summary of different equations with respect to multilayer adsorption can be found, e.g., in [1]. However, the standard BET equation remains the most important one. The standard BET equation is

$$\frac{v}{v_m} = \frac{cx}{(1-x)(1+cx-x)} \tag{1}$$

where v is the adsorbed moisture content (in the case of water vapor), v_m is the so-called monolayer capacity (the moisture content corresponding to that the first layer of the material surface is fully occupied), c is a constant related to the energy of adsorption and x is the relative pressure (humidity). To derive the standard BET equation, it is assumed that only the molecules in the first layer have a condensation heat that is different from that of the bulk water and that the heat of condensation in the second and higher adsorbed layers are equal, which is the same as the heat of liquefaction [3, 12]. Johannesson [13] further studied the assumption regarding the heat of condensation, the assumption

being modified so that both the condensation heat of the water molecules on the first layer and second layer are different from that of the normal bulk water while the water molecules on the third and higher layers have the same condensation heat as that of bulk water. By introducing this new assumption and combining other assumptions which are also made in obtaining the standard BET equation, a new equation, designated as the two-layer BET equation, can be obtained as

$$\frac{v}{v_m} = \frac{cx[1 + (b-1)(2x - x^2)]}{(1-x)[cx^2(b-1) + (c-1)x + 1]} \tag{2}$$

where there is one more constant parameter b accounting for the modified assumption concerning the condensation heat compared with the standard BET equation. With the help of a so-called sorption calorimeter [14, 15], it is possible to study the assumptions regarding the heat of condensation of the water on different layers. Johannesson [13] conducted detailed studies by comparing the measured differential heat of adsorption and the predicted value based on the standard BET equation and the two-layer BET equation for different porous materials. The results showed a better agreement between the measured differential heat of adsorption and the value predicted based on two-layer BET equation compared with that obtained by using the standard BET equation. It was concluded that the assumptions about heat of condensation behind the two-layer BET equation is more adequate compared with that using the standard BET equation.

Guggenheim [16], Anderson [17] and de Boer [18] modified the standard BET equation by assuming that the heat of condensation of the water molecules on the second and all the higher layers are the same, but different from that of bulk water, and a good agreement was found between the experimental data and the modified equation on different tested adsorbates. The modified equation is the so called GAB equation [19], which is

$$\frac{v}{v_m} = \frac{ckx}{(1-kx)[1 + (c-1)kx]} \tag{3}$$

Similar to the two-layer BET equation, there is one more constant, k, as compared to the standard BET equation. The property k is related to the modified assumption about the condensation heat compared with the standard BET equation.

Dent [20, 21] conducted some related studies and further discussed that the heat of condensation could actually differ for each layer, but the difference between the second and higher layers tends to be small. In addition, the mathematical complexity would be increased considerably if each of the layer was treated differently. Thus, for simplicity it was assumed that water molecules on the second and all the higher layers have the same condensation heat but different from that of bulk water. The Dent equation is based on the same principles as the GAB equation and also has the same mathematical form. It should be mentioned that Brunauer et al. [22] introduced an extension of the BET equation using a parameter k, whose value represents a measure of the attraction force of the adsorbent. Although the basis is quite different, Brunauer et al. arrived at an equation identical to the GAB equation. Thus, it might be reasonable to think that the parameter k may not only be related to the heat of condensation but also to other factors , e.g., the attractive forces.

1.2. The thickness of the adsorbed layer

In order to calculate the pore size distribution according to the BJH model, it is necessary to know the thickness of the adsorbed layer. As we know, the BJH model assumes two types of water, i.e., the adsorbed water and the capillary condensed water [4]. However, the sorption measurement itself cannot distinguish the two types of water and only measures the total moisture content at a given

relative humidity (RH). That is, the thickness of the adsorbed layer of water needs to be determined beforehand in the calculation of a pore size distribution.

It is often assumed that the statistical thickness of the adsorbed layer on a solid surface is a function of the relative humidity and the plot of this function is normally called the $t-$curve. The $t-$curve can be obtained by using the volume of the moisture adsorbed on the surface of an adsorbent divided by the surface area as

$$t = (V_{ad}/S) \cdot 10^{-3} \tag{4}$$

where t is the statistical thickness of the adsorbed layer in nm, V_{ad} is the adsorbed volume on the surface in $\mathrm{cm}^3 \cdot \mathrm{g}^{-1}$ and S is the surface area in $\mathrm{m}^2 \cdot \mathrm{g}^{-1}$. There is no direct means to obtain the exact surface area S of a material, and normally the BET specific surface area is used instead due to its wide application, e.g., in [23, 24]. It should also be noted that there are some discussions on to which extent the BET specific surface area represents the true geometrical surface area of a studied material [25]. More related discussions regarding this will be presented in Section 3. As mentioned earlier, the moisture content measured on a porous material during an absorption experiment at a relatively high RH contains both the adsorbed and the capillary condensed water and therefore it is not possible to obtain the V_{ad} directly from the measured data. For most cases, the standard BET equation predicts too high moisture content for adsorption at high RHs (as will be demonstrated later, the two-layer BET equation and the GAB equation have the similar weakness), thus it is not relevant to use this kind of prediction in the whole relative humidity range. Therefore, $t-$curves are often determined experimentally from nonporous adsorbents, where the capillary condensation is considered absent. Initially it was argued that a universal $t-$curve existed for all nonporous materials. This argument was later revised and it was proposed that the $t-$curve should be a function of the physicochemical and thermodynamic nature of the sample surface which can be interpreted in terms of the constant c obtained from analyzing the standard BET equation, e.g., in [23].

Numerous $t-$curves have been proposed for nitrogen adsorption and a review in this aspect can be found, e.g., in [1, 26]. As far as water vapor is concerned, Hagymassy et al. [9] studied the adsorption behavior on several types of adsorbents, such as silica gel, rutile and quartz and generalized four $t-$curves based on the different calculated energy constants c using the standard BET calculation. These types of $t-$curves are commonly used for determining the pore size distribution using water vapor. Apart from the $t-$curves proposed by Hagymassy et al., there are some other suggestions. The empirical Halsey equation has been used, e.g., see [27, 28]

$$t = -d(\frac{A}{\ln\phi})^B \tag{5}$$

where d is the thickness of a monolayer water molecules, ϕ is the relative humidity, A and B are constants. Espinosa and Franke [25] adopted an empirical equation accounting for the $t-$curve as

$$t = 0.395 - 0.189\ln(-\ln\phi) \tag{6}$$

By noting the commonly occurring overestimation of the adsorbed moisture content as predicted by the standard BET equation at high relative humidities (the predicted moisture content often ends up with infinity), Johannesson [12], in the context of pore size distribution calculations, assumed that only the water molecules in the first and second layer are considered in calculating the thickness of the adsorbed layer. Following this concept, the moisture contents in the first and second layer can be calculated based on the equations accounting for multilayer adsorption, e.g., using the standard or the two-layer BET equation, and then they can be used to calculate the $t-$curves using

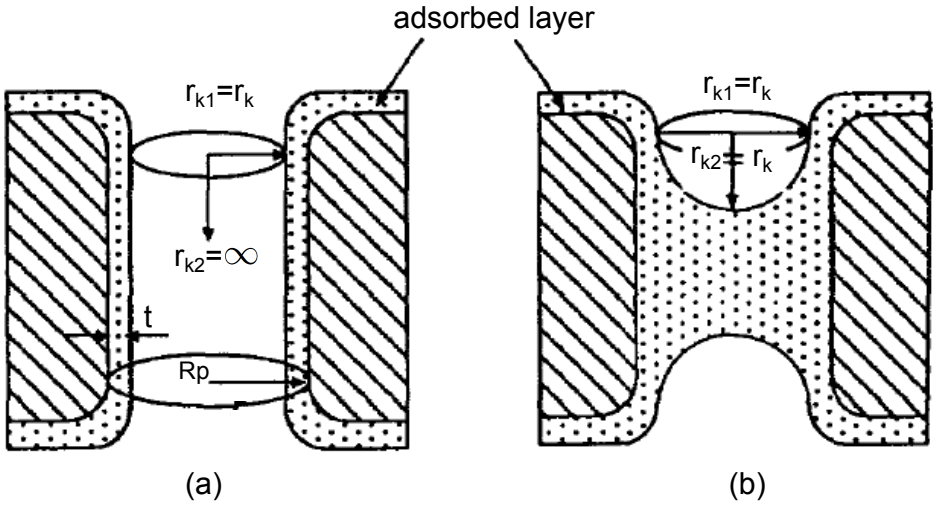

Figure 1: One proposed hypothesis explaining the hysteresis: different radii of the curvature during absorption (a) and desorption (b) for a cylindrical pore, slightly modified based on [1].

$$t = d \cdot \frac{v_1 + v_2}{v_m} \tag{7}$$

where v_1, v_2 and v_m are the calculated moisture content in the first layer, the second layer and the monolayer capacity, d is the thickness of a monolayer water molecules. The thickness of the first two layers are to be added to the calculated Kelvin radii at a certain relative humidity to obtain the radii of the studied pores. It should be mentioned that the calculation of the $t-$curves using this method is a somewhat crude approximation, but it has the advantage that the $t-$curves for an adsorbate on an adsorbent can be determined directly from the measured absorption data without considering any additional reference data. This is of interest since the adsorption behavior could be unique for an adsorbate combined with a certain adsorbent. The comparisons of different adopted $t-$curves for the studied materials will be presented later.

1.3. Sorption hysteresis

Sorption hysteresis refers to the phenomenon that the absorption isotherm follows a different path compared with the desorption isotherm, leaving a hysteresis loop between the two isotherms. The hysteresis phenomenon has attracted significant attention, e.g., see [1, 2, 29–31], and some recent progress can be found, e.g., in [32, 33]. The origin of the hysteresis phenomenon has not been fully understood yet. It is, however, generally agreed that the hysteresis is associated with capillary condensation [2]. The detailed discussion of the origin of the hysteresis phenomenon is beyond the scope of this work, with only two representative explanations which would have an important impact on the pore size distribution determination being introduced.

One proposed explanation for the hysteresis is based on the hypothesis that the curvature radii of the same pore are different during the absorption and the desorption, e.g., see [1]. The Kelvin equation is used to determine the radius of a curvature of capillary condensation and it can be related to the

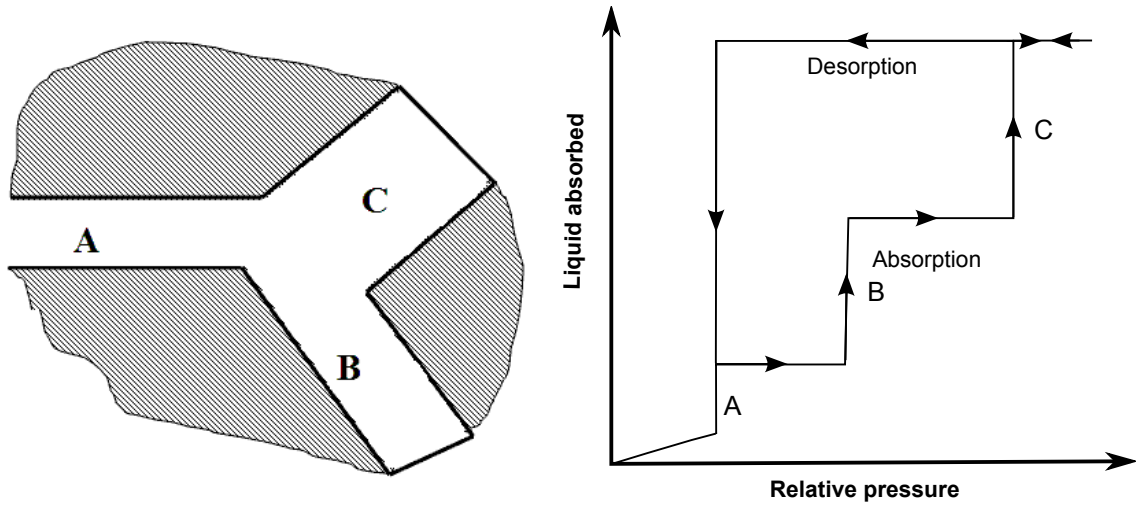

(a) (b)

Figure 2: An illustration of the proposed pore network concept accounting for hysteresis: (a) a pore system of three pores forming a network in a porous material, slightly modified based on [38] and (b) the corresponding schematic absorption and desorption isotherms, where the desorption isotherm is always higher than the absorption during the relative pressure range of capillary condensation of the three pores.

radii at the two principal directions r_{k1} and r_{k2}, which can be written as

$$\frac{1}{r_{k1}} + \frac{1}{r_{k2}} = -\frac{RT\rho_w}{M_w\gamma_w}\ln(\phi) \tag{8}$$

where M_w, γ_w and ρ_w is the molecular weight, surface tension of the liquid-gas interface and the density of water respectively, R is the gas constant and T is the temperature in Kelvin degree. Figure 1 schematically shows the concept considered for a cylindrical pore. According to this hypothesis, during absorption $r_{k1} = r_k$ and $r_{k2} = \infty$; while during the desorption, $r_{k1} = r_{k2} = r_k$. By inserting these relations into Eq.8, one obtains that the relative humidity for capillary condensed water in absorption (denoted as ϕ_A) and in desorption (denoted as ϕ_D) are different in the same pore, the relation being $\phi_D = \phi_A^2$. That is to say, for the same amount of moisture content, $\phi_D < \phi_A$. Thus, the desorption curve is by the model predicted to be above the the absorption curve during a hysteresis loop. The author [1] further extended the applicability of the same concept to other pore shape assumptions, including ink-bottle pores, parallel plate (slit) pores and wedge shaped pores. It was concluded that the relation as derived, i.e., $\phi_D = \phi_A^2$, also holds for the different pore models.

Following the concept of the above explained model, the hysteresis between the absorption and desorption curves would be an intrinsic property of porous materials during the sorption measurements, meaning it will show up as long as capillary condensation takes place. However, it must be noted that there are some studies [34–37] which did reveal that well defined reversible Type IV isotherms (IUPAC classification) are obtainable on a model mesoporous material MCM-41, without showing any hysteresis at all. Taking into account the reversibility of the absorption and the desorption isotherms for mesoporous materials, it seems that the hypothesis assuming different radii of the meniscus curvature in the absorption and desorption is not applicable in explaining the hysteresis phenomenon.

Another proposed approach which is called network theory or pore-blocking concept attributes the

hysteresis to the inter-connectivity of the pore system, e.g., see [1, 38]. An illustration of this model can be given by looking at a simplified pore system with three pores forming a network as shown in Figure 2a. The pore size of the three pores decreases in the sequence of pore C, pore B and pore A. Pore B and pore C are closed at one end. During the absorption, the vapor will enter and condensate in the pores in the sequence of pore A, pore B and pore C. Even though the small pores are filled first, they do not block off what is happening in the internal big pores closed at one end and the big pores can be filled through evaporation from the end connecting with small pores [1]. When the absorption process is finished at a certain relative pressure, all the three pores are filled with the liquid. During desorption, as the relative pressure decreases, theoretically the liquid in pore C should be vaporized and emptied first and after this, pore B and pore A will be emptied, which is the opposite process of the absorption process described previously. However, the liquid in pore B and pore C cannot vaporize at their condensation pressure because the liquid is not in contact with the vapor phase and the liquid in pore B and pore C will be under a metastable condition. When the relative pressure decreases to the condensation pressure of pore A, the liquid in pore A will vaporize and the liquid in both pore B and pore C will also vaporize at this point since they are no longer blocked by the liquid in pore A. That is, during desorption, the liquid in the three pores will vaporize at the same relative pressure, i.e., the condensation pressure for pore A in this case. This will result into that the moisture content measured during the desorption at the relative pressures higher than that of the condensation pressure of pore A will always be higher than the moisture content measured during the absorption, i.e., resulting into a hysteresis loop, the isotherms being schematically shown in Figure 2b. The network effect is also mentioned sometimes as the pore blocking effect, e.g., in [31, 39]. The controlling pore size of the network, e.g., pore A in this case, can be referred to as the entry or neck size [40, 41] in the context of porosity description. It should be mentioned that it is not appropriate to treat this network effect absolutely the same as that caused by the so called "ink-bottle" pores, since the network effect depicts the complex pore structure in the three dimensional space while the concept of "ink-bottle" pores provides a too simplified picture in this regard as discussed by, e.g., Sing et al. [2].

With the above mentioned network hypothesis, it is straightforward to explain the reversibility of the absorption isotherm and the desorption isotherm for a given porous material, which cannot be explained by the previously described hypothesis assuming different radii of the meniscus curvature in the absorption and the desorption, as illustrated in Figure 1. No hysteresis simply indicates the absence of any pore blocking effect in the porous material. In this sense, it seems more reasonable to assume that the network theory is more relevant in explaining the hysteresis phenomenon compared with that assuming different meniscus curvature radii in absorption and desorption. This argument is somewhat supported by the discussions in, e.g., [24, 39], claiming that the sorption hysteresis is only a "short term" phenomenon and it will disappear given a long enough time.

Porosity characterization using water vapor measurements has been studied for a while. However, the analysis of sorption data is somewhat inconsistent in literature due to some non-fully solved factors, e.g., the ones discussed above. In this work, the impact of using different equations proposed for multilayer adsorption on the calculated specific surface area will be studied. The influence of the different $t-$curves on the derived pore size distribution will also be discussed and the pore size distribution will be derived from both the absorption and the desorption isotherms. Additionally, the network theory will be demonstrated as a concept of particular interest in explaining the differences found between the absorption and desorption measurements and the properties derived from the absorption and the desorption isotherm of the studied porous materials.

Table 1: Properties and the chemical composition of the two cements used in this study.

		CEM I (CEM I 32.5 R)	CEM III (CEM III/B 42.5 N)
Density	(g/cm^3)	3.06	2.90
Fineness	(cm^2/g)	2905	4635
Water demand	(%)	26.2	32.3
Initial setting time	(min)	185	270
Loss on ignition	(%)	2.1	1.4
SiO_2	(%)	20.6	29.2
Al_2O_3	(%)	5.6	8.9
Fe_2O_3	(%)	2.4	1.2
CaO	(%)	63.4	48.0
MgO	(%)	1.6	4.8
SO_3	(%)	2.9	2.6
K_2O	(%)	0.7	0.6
Na_2O	(%)	0.2	0.2
Cl	(%)	<0.1	<0.1

2. Experimental

2.1. Materials

Three materials were studied in this investigation: one model mesoporous material MCM-41 and two types of hardened cement pastes. The primary purpose of including the model material in this investigation is to validate the applicability of sorption measurement using water vapor in the context of surface area and porosity determination.

MCM-41 is a silica based material and its pore structure is in the form of hexagonal arrays of uniform tubular channels of controlled width. Of this reason, MCM-41 is often used as a model material in porosity studies. The MCM-41 used in this study is produced by Tianjin Chemist Scientific Ltd. The nominal pore diameter provided by the producer is 3.0 nm and the nominal specific surface area and the total pore volume is reported to be $\geq$ 800 m^2/g, $\geq$ 0.70 ml/g respectively.

Two different cements, i.e., CEM I 32.5 R and CEM III/B 42.5 N, were used to prepare the paste samples with a W/C ratio of 0.4. Table 1 shows the properties and the chemical composition of the two cements used. A paddle mixer was used for the mixing of the fresh samples. After mixing, the pastes were cast into plastic vials with a diameter of about 15 mm and a length of about 50 mm with proper compaction. After one day of sealed curing at room temperature (about 20 °C) in the plastic vials, the paste samples were demoulded. Then, each paste sample was placed into a bigger self-sealable plastic flask filled with saturated lime water for curing at room temperature till the desired age for experiments.

The hardened cement paste samples were cured for about 6 months before the sorption measurements. The "dynamic vapor sorption" (DVS) method was used to do the sorption measurements (Section 2.2). Since the sample size which can be used in a DVS instrument is relatively small, it normally means that the hardened cement paste samples need to be crushed and/or even grinding. In some cases, the representativeness of the sample can be questioned. However, it is normally possible to collect a large representative sample and then divide them into a fine powder-like mass. One may also argue that the crushing of a sample might cause the change of the porosity. As the adsorption and capillary condensation studied in this context is at the nanometric scale, it is believed that the

crushing of samples has very little or no effect at all in changing the nanometer porosity, e.g., as illustrated experimentally in [24, 42].

The cylinder samples of the hardened cement pastes were firstly vacuum saturated with saturated lime water and then the crushing and grinding of the samples was conducted in a carbon dioxide free chamber to avoid carbonation. Meanwhile, to avoid possible drying of the samples during the preparation process, the RH inside of the chamber was set at 1 (the measured RH was about 0.90–0.95) and the sample crushing and grinding was conducted rather quickly (in 30–40 min) for each paste. Immediately after that, the ground sample powders were placed into plastic flasks containing saturated lime water with the amount just to cover the powders (for about a week) before the sorption experiments. This procedure was also conducted in the carbon dioxide free chamber. More discussions about the sample preparation can be found in [43].

The hardened cement pastes will be shortly designated as CEM I and CEM III in the following description.

2.2. Sorption measurements

The DVS method was used to study the sorption behaviors of the three porous materials under consideration. The measurements were conducted in a climate incubator where the temperature can be regulated and controlled. The relative humidity was generated into desired proportions by mixing two air flows, i.e., a totally dry (RH = 0) and a totally saturated (RH = 1) air. The proportions of the two flows can be accurately controlled by the flow regulator devices. Figure 3 shows the instrument schematically. The sample was placed into a sample holder at one end of a microbalance. A reference holder, which is symmetrically connected to the sample holder on the other end of the microbalance, was used with the purpose to eliminate the effect of the vapor adsorption on the surface of the sample holder.

One advantage of the DVS method is that the RH can be programmed to vary arbitrarily during a measurement. Additionally, the sample size used in a DVS instrument is often very small, which is on the order of several to tens of milligram (mg). This enables the equilibrium conditions to be achieved rather quickly. It is also of interest to note that the mixed vapor is free of carbon dioxide, which makes this method suitable to study cement based materials, e.g., see [44, 45].

It should be noted that it could take a very long time for the equilibrium condition to be established at a given RH. Actually, it is practically impossible to wait for the establishment of the exact equilibrium condition at each RH in a sorption measurement. The duration time of each RH in the DVS instrument can be controlled by either setting the mass change ratio against time, dm/dt, or setting the duration time directly. Once the set conditions are met, the instrument will directly go to the next step of the set RH scheme. In this study, the dm/dt is set as 0.002% and the shortest and the longest duration time for each step is set to be 0.5 and 24 hours, respectively. The moisture content corresponding to each measured RH will be then extrapolated from the measured data and the details will be presented later. The temperature of the measurements was 25 °C.

The sorption measurement for the model material MCM-41 (as received) in this study started from an absorption (RH from 0 to 0.95) followed by a desorption process (RH from 0.95 to 0). Discussions concerning the possible damage of cement samples when the RH decreases to some low values (typically 0.3-0.4) can be found, e.g., in [24, 46]. Due to this, the experiments with hardened cement paste samples started from the desorption and then followed by the absorption. The purpose of the above described approach is trying to reduce the possible effect caused by the so-called drying damage at low RHs. A more detailed discussion in this aspect will be conducted later combined with the measured experimental data.

The same type of sorption measurement was conducted three times using different samples on the model material MCM-41 and the two hardened cement pastes in this study. The total experimental

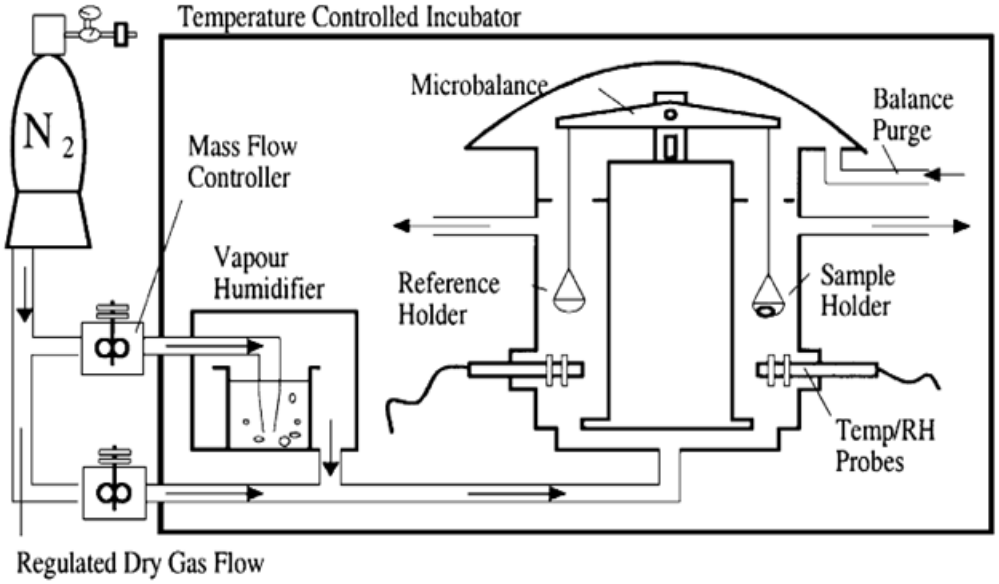

Figure 3: Schematic illustration of a dynamic vapor sorption (DVS) instrument. Dry and saturated air are mixed to generate the desired relative humidity and a symmetric reference holder is used to counteract the adsorption on the sample holder [12].

sorption study lasted for about four months and the sampling of the three measurements were chosen in the beginning, the middle and the end of the total measuring time. By doing so, firstly the repeatability of the instrument can be tested as the model material MCM-41 has a stable pore structure (which will not change against time); and secondly the possible evolution of the pore structure against time for the hardened cement paste samples can also be checked since further hydration might take place in cement based materials in the presence of moisture even though some relatively old samples are used. A more detailed discussion about the measurements of the materials under study is presented elsewhere [43].

3. Results and discussion

3.1. Sorption isotherms

As discussed before, it is practically impossible to wait for the establishment of the exact equilibrium condition at each studied RH step. Therefore, a data processing procedure (curve fitting) is adopted to extrapolate the sample mass so as to represent the equilibrium condition. The sample mass against time in a sorption measurement has been proposed following the equation [47, 48]

$$m(t) = m_f - (m_f - m_0)\mathrm{e}^{-k(t-t_0)} \tag{9}$$

where $m(t)$ is the sample mass at the time t, m_0 represents the initial mass and t_0 is the initial time of the curving fitting, m_f is the fitted asymptotic sample mass at the equilibrium condition for the studied RH and k is a curve fitting constant. Figure 4 shows an example of the extrapolation. The solid line represents the measured data in the experiment, and the dash-dot line is the fitted curve

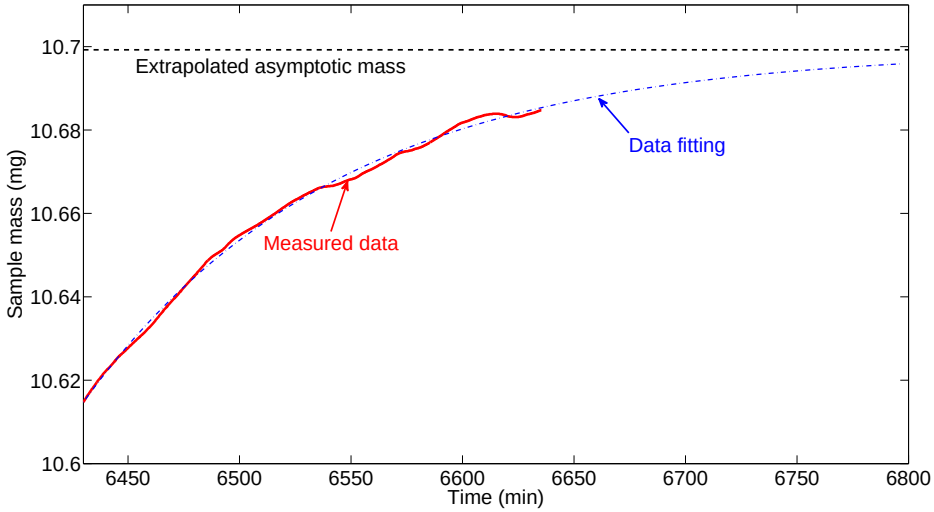

Figure 4: An example showing the data processing procedure to extrapolate the asymptotic sample mass at the equilibrium condition.

and the dot line shows the final extrapolated asymptotic sample mass at the equilibrium condition for the RH step considered.

With the extrapolated data, the corrected isotherms under equilibrium conditions can be constructed. For the sample MCM-41, besides the point at RH = 0, the point with some difference between the extrapolated and the measured isotherms is found at RH = 0.5 in desorption and RH around 0.6 in absorption where moisture condenses/desorbs drastically. For the hardened cement paste samples CEM I and CEM III, the point at RH = 0 is also a point with rather significant difference between the extrapolated and the measured isotherms, which is similar to the sample MCM-41. Additionally, more points with important difference between the extrapolated and the measured desorption isotherms are found at the very high RHs (0.95, 0.9 and sometimes 0.8) of the studied hardened cement paste samples. The reason has been discussed already, i.e., due to the experimental procedure and the pre-setting in the instrument. For the other RH points, the relative difference of the moisture content between the extrapolated and measured data are no more than about 0.5%.

The corrected sorption isotherms of the three studied materials are presented from Figure 5 to Figure 7. Compared with the corrected sorption isotherms of the model material MCM-41, the hysteresis at low RHs is found for the two hardened cement paste samples. The hysteresis at low RHs was reviewed and shortly discussed in [8], arguing that this hysteresis is due to the fact that the thermodynamic equilibrium is still not established at low RHs during absorption. Since the extrapolation process is adopted and the absence of the hysteresis at low RHs in the corrected isotherms of the sample MCM-41, it may indicate that the non-equilibrium assumption is not relevant in this context. However, the hysteresis at low RHs can be better explained if the network theory is considered, which is that higher moisture content measured during the desorption compared with that during absorption is caused by the aforementioned pore-blocking effect. The comparison between the model material MCM-41 and the hardened cement paste samples indicates that the pore-blocking effect may disappear in the MCM-41 at low RHs, while it lasts almost for the whole measured RHs for the hardened

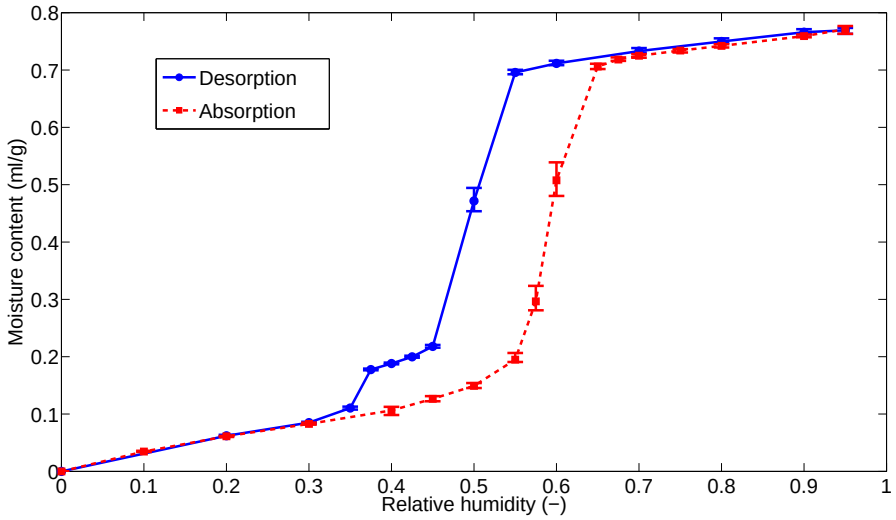

Figure 5: The sorption isotherms for the MCM-41based on the extrapolated data at equilibrium conditions and the error bar shows the variation of three different measurements. The moisture content is expressed as ml water per gram of dry sample and the mass of the dry sample is determined at the point where RH = 0.

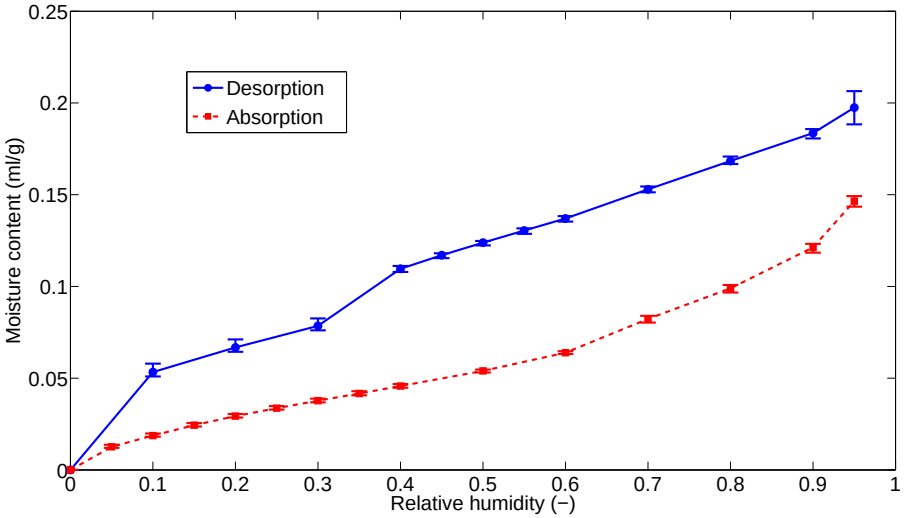

Figure 6: The sorption isotherms for the paste CEM I based on the extrapolated data at equilibrium conditions and the error bar shows the variation of three different measurements. The moisture content is expressed as ml water per gram of dry sample and the mass of the dry sample is determined at the point where RH = 0.

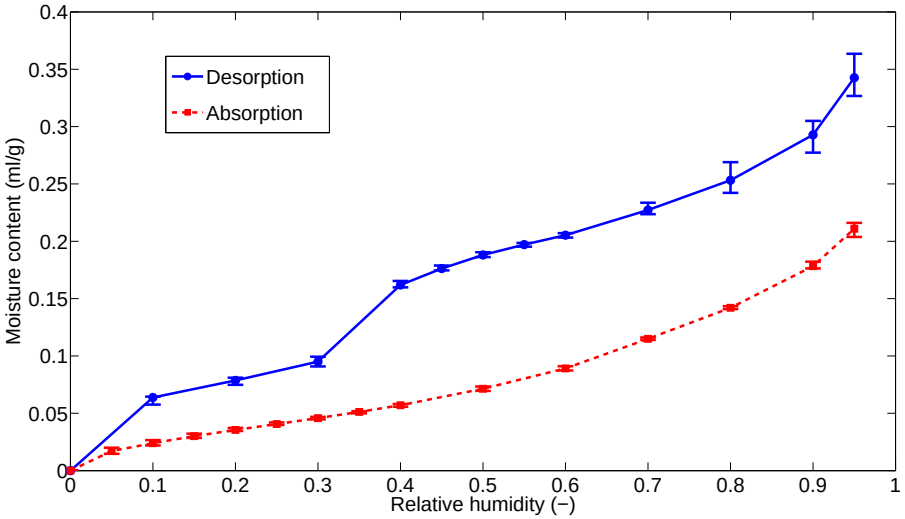

Figure 7: The sorption isotherms for the paste CEM III based on the extrapolated data at equilibrium conditions and the error bar shows the variation of three different measurements. The moisture content is expressed as ml water per gram of dry sample and the mass of the dry sample is determined at the point where RH = 0.

cement paste samples, which might possibly imply a much more complex pore structure including pore-blocking effect in the hardened cement paste samples.

3.2. Specific surface area of the studied materials

The specific surface area S (m^2/g) is proportional to the amount of the adsorbed moisture on the first monolayer when it is completely covered, with the expression given as

$$S = \frac{A_m N_A}{M_w} v_m \tag{10}$$

where v_m is the monolayer capacity (g/g), $N_A = 6.02 \cdot 10^{23}$ (mol^{-1}) is the Avogadro constant, $M_w = 18.0$ (g/mol) is the molar mass of water and $A_m = 10.6$ (Å^2) is the area occupied by one water molecule [9] . By inserting these values, Eq.10 can be written as

$$S = 3540 \cdot v_m \tag{11}$$

As has been discussed earlier, several different equations have been developed to describe the multilayer adsorption. If different types of equations accounting for multilayer adsorption are used, the calculated specific surface area could be different. In this section, the standard BET equation, the two-layer BET equation and the GAB equation will be used to calculate the specific surface area. The absorption data from Figure 5 to Figure 7 in the RH range ≤ 0.4 are used to do the necessary curve fitting to obtain the important parameters.

The curve fitting results are shown from Figure 8 to Figure 10. It can be observed that for the MCM-41 (Figure 8), the predicted amount of the adsorbed moisture content decreases in the sequence of the standard BET equation, the two-layer BET equation and the GAB equation and the predicted isotherms all lie below the measured moisture content at the RH between 0.5 to 0.9. For the hardened

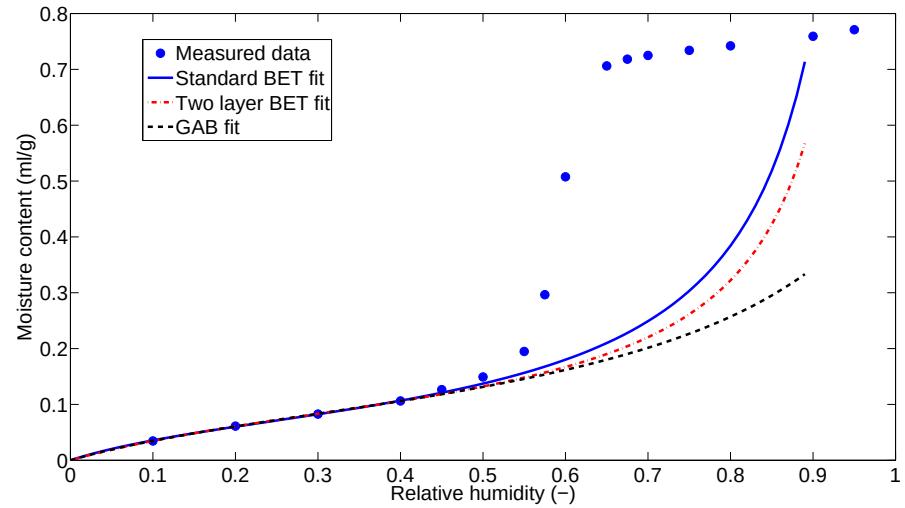

Figure 8: The curve fitting for the MCM-41 using the standard BET equation, the two-layer BET equation and the GAB equation accounting for multilayer adsorption.

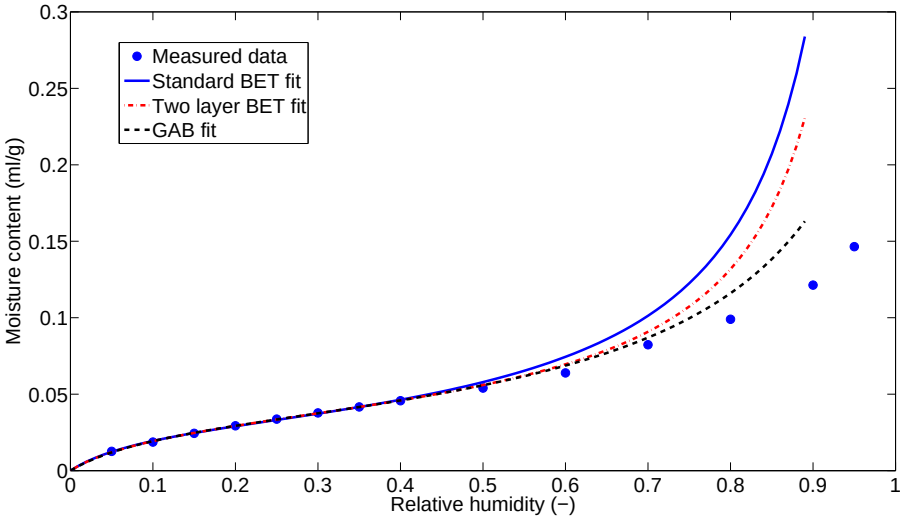

Figure 9: The curve fitting for the paste CEM I using the standard BET equation, the two-layer BET equation and the GAB equation accounting for multilayer adsorption.

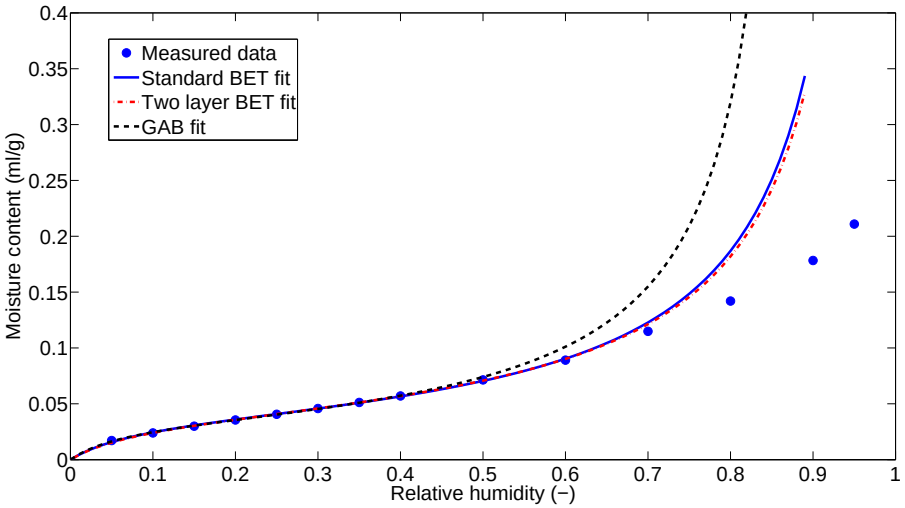

Figure 10: The curve fitting for the paste CEM III using the standard BET equation, the two-layer BET equation and the GAB equation accounting for multilayer adsorption.

cement paste sample CEM I (Figure 9), the predicted amount of the adsorbed moisture content decreases in the same sequence as that of the MCM-41 but all of the predicted adsorption isotherms are higher than the measured absorption isotherms at the RH $>$ 0.5. As introduced before, the measured absorption isotherm contains both the moisture uptake from the multilayer adsorption and the capillary condensation. Thus, the moisture content through multilayer adsorption should always be lower than the measured absorption data. Therefore, all the three equations for multilayer adsorption tend to overestimate the adsorbed moisture content at the RH $>$ 0.5. The similar overestimation of the adsorbed moisture content at high RHs is also observed for sample CEM III (Figure 10). However, for CEM III, the GAB fit results in the highest isotherm which is different compared with the results obtained for the sample MCM-41 and CEM I. This is related to the nature of the GAB fitting parameters k. The calculated specific surface area based on the three different equations and the fitted parameters are shown in Table 2.

According to results presented in Table 2, it can be found the calculated specific surface area based on the two-layer BET equation is normally smaller than that based on the standard BET equation. The relative difference for the MCM-41 and the paste CEM I are 26% and 24% respectively, while the relative difference is much smaller for the paste CEM III (less than 1%). The specific surface area calculated from the GAB equation is bigger than that from the standard BET equation for the MCM-41 and the paste CEM I while the opposite relation is found for the paste CEM III. This is associated with the best fitted GAB parameter k. The k value for both MCM-41 and CEM I are less than 1 while the value for CEM III is larger than 1. It has also been noticed that the values for k in literature is often reported to be less than 1, e.g., see [21, 49]. Thus, unsurprisingly it can be concluded that the calculated specific surface area is very sensitive to which equation (model) is used for multilayer adsorption. It should be noted that it has been claimed that the calculated specific surface area actually does not represent the real geometrical surface area [25], because it also depends on the interaction forces between the adsorbate and the adsorbent, which are reflected in the values of the parameters like c, b and k as presented in Table 2.

Table 2: The fitted parameters and the calculated specific surface area for the studied materials based on different equations accounting for multilayer adsorption.

	MCM-41			CEM I			CEM III		
	BET[a]	TBET[a]	GAB	BET[a]	TBET[a]	GAB	BET[a]	TBET[a]	GAB
v_m	0.0800	0.0591	0.0994	0.0315	0.0239	0.0346	0.0381	0.0357	0.0346
c	6.04	7.12	5.40	11.17	14.37	10.51	12.24	12.60	13.61
b	-	2.45	-	-	2.51	-	-	1.28	-
k	-	-	0.81	-	-	0.89	-	-	1.12[b]
surf. area (m^2/g)	283	209	352	112	85	123	135	126	123

Note: (a) BET and TBET represent the standard BET equation and the two-layer BET equation respectively; (b) the k value is often reported as less than 1.

3.3. Pore size distribution of the studied materials

3.3.1 The thickness of the adsorbed layer

Different models to calculate the thickness of the adsorbed layer of water vapor, or the $t-$curves, have been discussed previously. The impact of the model selected on the calculated thickness of the adsorbed layer is discussed in the following. The Halsey equation and the empirical equation Eq.6 are two types of $t-$curves for water vapor, which are independent of the adsorbents under consideration. The $t-$curves proposed by Hagymassy et al. [9] for water vapor depends on the standard BET constant c. The BET constant c values for the proposed four generalized $t-$curves are c =10−14.5, c =50−200, c =5.2 and c =23. Three other $t-$curves are also included following the assumption made by Johannesson [12] for comparison purpose, i.e. only the water molecules in the first and second layer as calculated will be considered to account for the thickness of the adsorbed layer (referring to Eq.7), based on the standard BET equation, the two-layer BET equation and the GAB equation. They are denoted as J-BET, J-TBET and J-GAB, respectively.

The comparison between the different $t-$curves for the studied materials MCM-41, CEM I and CEM III are shown in Figure 11, Figure 12 and Figure 13. The standard BET constant c calculated for the MCM-41 is about 6 (Table 2), thus the Hagymassy et al. $t-$curve with $c = 5.2$ is considered as the most relevant. The standard BET constant c calculated for the CEM I and CEM III are about 11 and 12 (Table 2), respectively. Therefore, the Hagymassy et al. curve with c =10∼14.5 is used for both CEM I and CEM III. Of all the $t-$curves considered, the Halsey equation predicts the highest values at low RHs (<0.4) and generally the Hagymassy et al. curve gives the highest values at high RHs. The three other $t-$curves, i.e., the J-BET, J-TBET and J-GAB, basically predict lower values compared to other $t-$curves especially when the RH is higher than 0.4. Since only the water in the first two layers as calculated based on the equations accounting for multilayer adsorption is considered to calculate the thickness of the adsorbed water and even though the equations tend to overestimate the moisture contents at high RHs, it is not surprising that the predicted thickness of the adsorbed layer from these three $t-$curves (J-BET, J-TBET and J-GAB) are relatively smaller compared with other $t-$curves considered in this study.

In order to demonstrate the impact of the assumed thickness of the adsorbed layer on the determined pore size distribution, the application of Kelvin equation without considering any adsorbed layer at all, i.e., $t \equiv 0$, will also be included in this study. The $t-$curves considered in the calculation of pore size distribution are listed in Table 3.

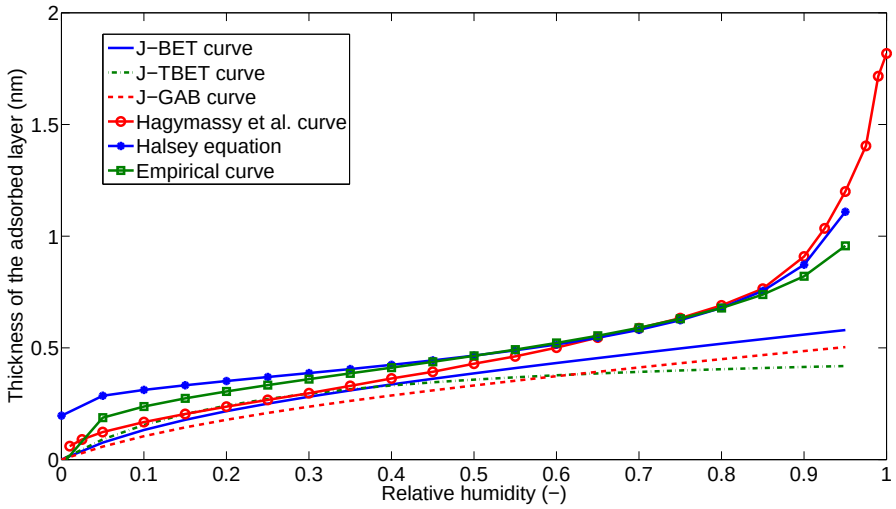

Figure 11: Different $t-$curves considered for the model material MCM-41.

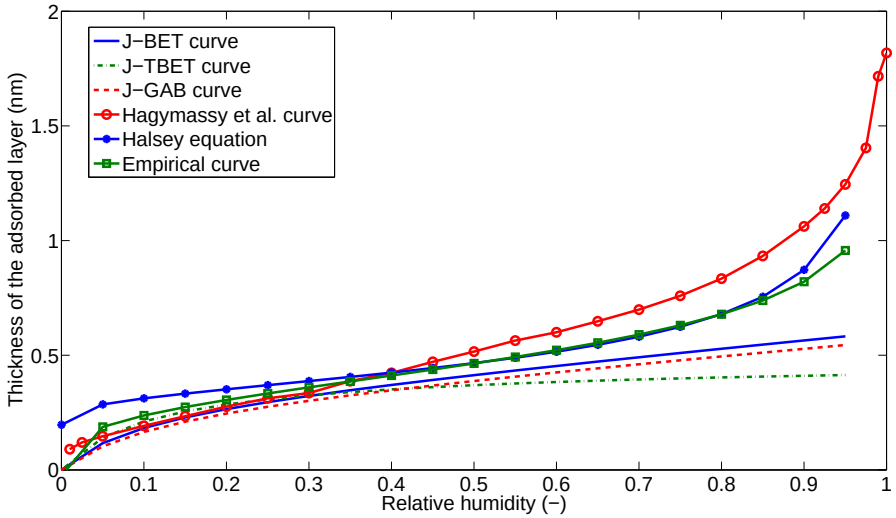

Figure 12: Different $t-$curves considered for the paste CEM I.

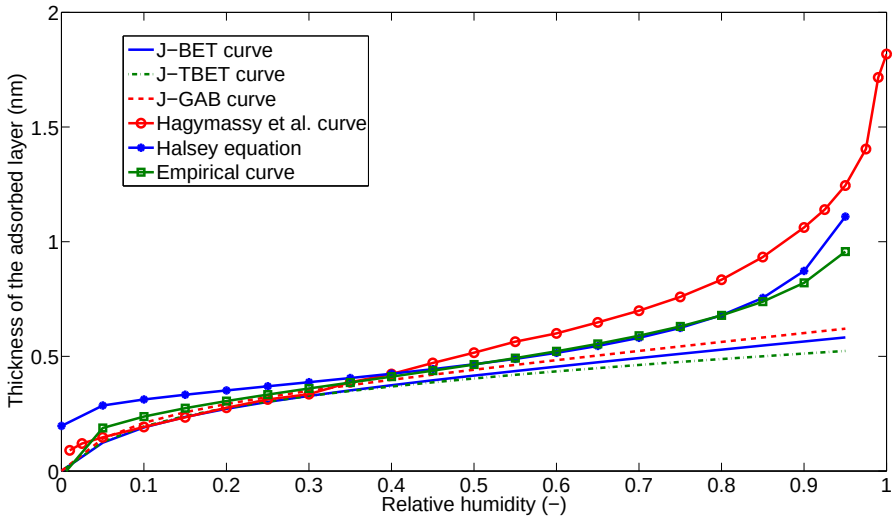

Figure 13: Different $t-$curves considered for the paste CEM III.

Table 3: The different $t-$curves considered in calculating the pore size distribution.

$t-$curves	Thickness t (nm)	Ref.
Kelvin-0 curve	$t \equiv 0$	-
Empirical curve	$t = 0.395 - 0.189\ln(-\ln\phi)$	[25]
Halsey equation	$t = -0.3(1.63/\ln\phi)^{1/3}$	[50]
Hagymassy et al. curve	Figure 11 to Figure 13	[9]
J-BET curve	Figure 11 to Figure 13	-
J-TBET curve	Figure 11 to Figure 13	-
J-GAB curve	Figure 11 to Figure 13	-

3.3.2 Pore size distribution

Following the BJH model, the pore volume of a studied material can be calculated using the moisture content data from high RH to low RH step by step. Thus, the total calculated pore volume depends on that to which RH value the calculation is executed. The lower the RH limit considered in the calculation, the bigger the calculated total pore volume. There is a possibility that the calculated pore volume will be bigger than the maximum measured moisture content if the lowest RH limit considered in the calculation is too low. That is because the calculation of pore size distribution using the Kelvin equation could only be applied in the RH range where capillary condensation takes place. At a certain low RH, capillary condensation could be absent for a studied material and the measured moisture content is merely due to multilayer adsorption. There is no general agreement on what is the limiting RH for capillary condensation in this type of calculations [8] and it has been indicated by some studies that the corresponding limiting pore size (width) may be as high as 7.5 nm [51, 52]. Normally, the closure point of the hysteresis is taken as the lower limit of capillary condensation [53]. However, the sorption data of the two hardened cement paste samples in this study show no obvious closure of the hysteresis. Therefore, from a practical perspective, the limiting pore size (the corresponding RH) in this study is determined by comparing the calculated total pore volume with the maximum moisture content measured. When these two values get sufficiently close to each other, the calculation is then terminated. In this manner, an indication of the lowest allowable RH is estimated. It should be noted that the estimated lowest allowable RH depends on the $t-$curve used in the calculation. The pore volume calculation also depends on the assumption concerning the pore shape. Cylindrical pores are assumed in the calculation described in this paper.

The calculated pore size distribution also depends on which isotherm is used as input data, i.e., desorption or absorption. There is no consensus about which isotherm should be adopted to calculate the pore size distribution. It is clearly stated in the IUPAC report dealing with sorption [2] that it is impossible to provide unequivocal recommendations in the absence of detailed knowledge about the geometry of the pores under study. But it seems to be more and more accepted that the calculation using absorption measurements may be more representative for the true pore size distribution while the calculation from the desorption perhaps is more related to the network effect (referring to the pore entry or neck sizes discussed before or the more simplified conventional "ink-bottle" model) [8, 39]. In this study, the pore size distribution will be calculated from both the absorption and desorption isotherms for comparison. It has been mentioned earlier that there is a hypothesis assuming different radii of the meniscus curvature for the same pore during the absorption and desorption, e.g., see Figure 1. However, this is considered as irrelevant for our purposes since it fails to explain the reversibility of the absorption and the desorption isotherms for mesoporous materials. Therefore, a hemispherical meniscus will be assumed in both desorption and absorption (referring to Figure 1b, $r_{k1} = r_{k2} = r_k$).

The calculated differential pore size distribution (PSD) curves of the MCM-41 from the desorption and the absorption isotherm using different $t-$curves are shown in Figure 14. It can be seen that the PSD curves calculated from the desorption isotherm using different $t-$curves (Figure 14a) basically have the similar shape with only one peak, except the one using Kelvin-0 $t-$curve which shows two peaks. The pore radii corresponding to the peak in the calculated PSD curves (except that using the Kelvin-0 $t-$curve), sometimes referred to as the most frequent pore radii R_{max} [26], are in the range of 1.7 nm to 1.9 nm, with the one using Halsey equation as the $t-$curve giving the biggest value and the one using the J-GAB $t-$curve giving the smallest. The two peaks in the pore size distribution curve using the Kelvin-0 $t-$curve corresponds to pore radii at about 1 nm and 1.4 nm. Similar trends are also found in the PSD curves calculated from the absorption isotherm using the six different $t-$curves (except that using the Kelvin-0 $t-$curve), as presented in Figure 14b, but the pore radii R_{max} are bigger than that calculated from the desorption isotherm (Figure 14a), which are in the range of 2.4

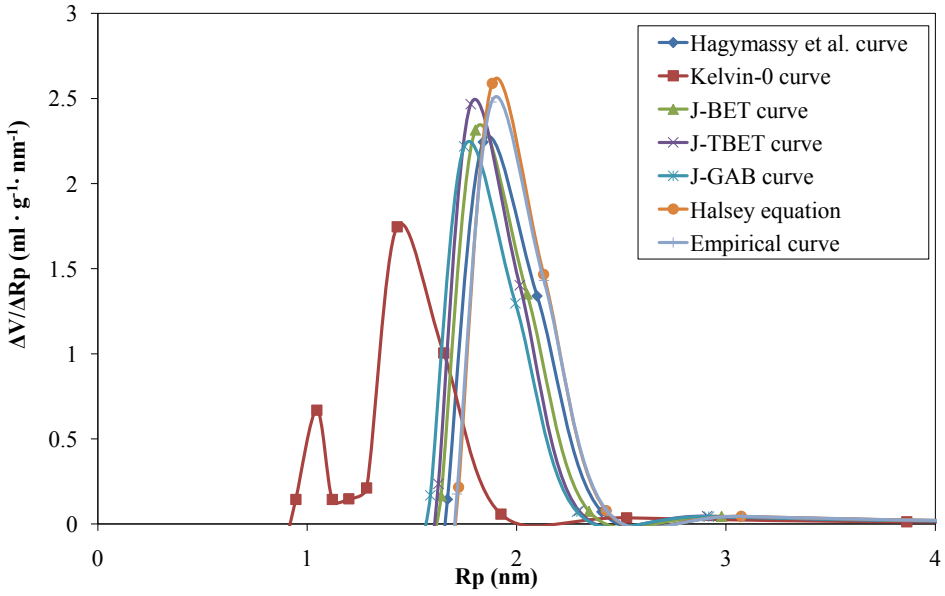

(a)

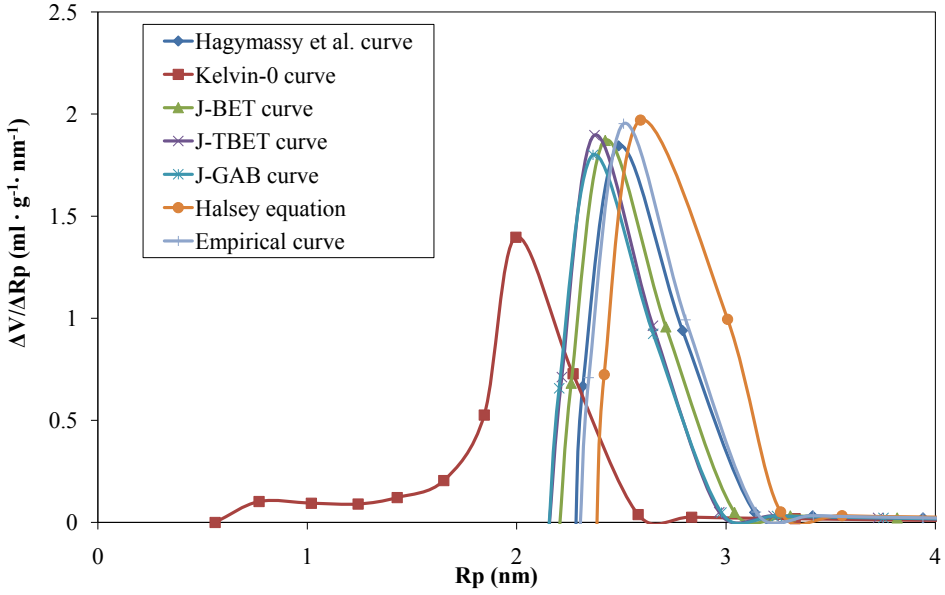

(b)

Figure 14: Differential pore size distribution of the MCM-41 calculated from (a) the desorption isotherm and (b) the absorption isotherm using different $t-$curves.

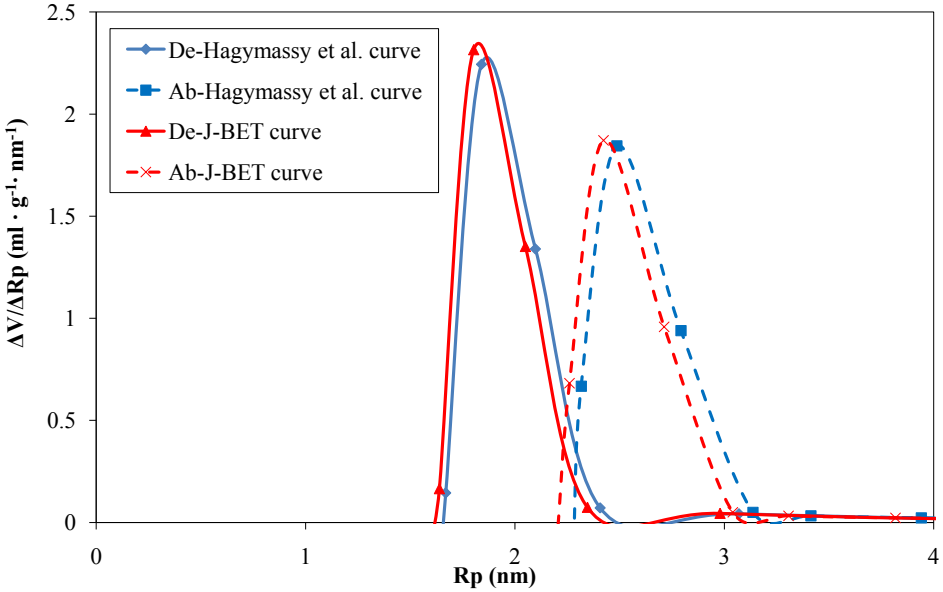

Figure 15: Comparison of the differential pore size distribution of the MCM-41 calculated from the desorption and absorption isotherms using Hagymassy et al. and J-BET $t-$curves.

nm to 2.6 nm. However, the PSD curves calculated from the absorption isotherm using the Kelvin-0 $t-$curve also shows one peak, whose corresponding pore radii is about 2 nm, but it has a relatively broad tail around the pore radii of about 1 nm.

Additionally, the PSD curves calculated from the absorption isotherm are slightly broader than those calculated from the desorption isotherm. A more representative comparison about the difference between the PSD curves calculated from the absorption and the desorption isotherms using Hagymassy et al. $t-$curve and J-BET $t-$curve is presented in Figure 15.

The influence of the assumed thickness of the adsorbed layer ($t-$curves) on the calculated pore size distribution can be summarized as follows: the thinner the layer is assumed, the smaller the pore size will be calculated. This becomes more evident by comparing the PSD curves calculated using either of the six other $t-$curves with that using the Kelvin-0 $t-$curve, see Figure 14.

Due to the restriction on the total pore volume adopted, the calculation of the PSD curves is terminated, e.g., when the pore radii are around 1.5-1.6 nm using the desorption isotherm (not considering that using the Kelvin-0 $t-$curve). That is because the calculated total pore volume is already equal to the maximum measured moisture content at the pore radii of 1.5-1.6 nm (corresponding to RH of around 0.4). The indication of this calculation can be understood as that the limiting RH (at the low end) for capillary condensation is about 0.4 for the model material MCM-41, and the moisture content measured under the RH of 0.4 is probably due to multilayer adsorption. However, the PSD calculation using the Kelvin-0 $t-$curve still continues under the pore radii (1.5-1.6 nm) since the total calculated pore volume is still much less than the maximum measured moisture content (as it does not account for the adsorbed water). It can be imagined that the adsorbed water is actually treated as the capillary condensed water in the very small pores when the Kelvin-0 $t-$curve is used, which causes the overestimation of the volume of the very small pores. This tends to motivate the statement that if the thickness of the adsorbed layer is underestimated, then the volume of the very small pores

Table 4: The calculated BJH surface area and the BET specific surface area for the MCM-41. The most frequent pore radii R_{max} with different $t-$curves are also presented.

Items		Surface area (m^2/g)		R_{max} (nm)	
		absorption	desorption	absorption	desorption
BJH	Hagymassy et al. curve	617	814	2.5	1.8
	Kelvin-0 curve	843	982	2.0	1.4
	J-BET curve	615	817	2.4	1.8
	J-TBET curve	613	834	2.4	1.8
	J-GAB curve	603	800	2.4	1.7
	Halsey equation	631	857	2.6	1.9
	Empirical curve	631	845	2.5	1.9
BET		283		-	

becomes overestimated, as clearly illustrated by the PSD curve using the Kelvin-0 $t-$curve compared with that using the other $t-$curves in Figure 14a.

It is of interest to compare the original measured desorption isotherm of the MCM-41 in Figure 5 with the obtained PSD curves (Figure 14a). There is a relatively sharp decrease or a shoulder after the RH at about 0.4 before the closure of the hysteresis. The peak around 1 nm in the determined PSD curve using the Kelvin-0 $t-$curve corresponds to this shoulder. However, if one looks into other PSD curves using a suitable $t-$curves, the calculation is actually terminated before this sharp decrease. Thus, it can be concluded that the peak around 1 nm in the PSD curve using the Kelvin-0 $t-$curve is just a calculation defect caused by not considering the adsorbed layer properly, which does not necessarily indicate the presence of another group of pores with radii around 1 nm in the MCM-41. The PSD curve calculated from the absorption isotherm using the Kelvin-0 $t-$curve (Figure 14b) results in no peak around 1 nm, which motivates the above statement.

One possible explanation for the existence of the shoulder before the closure of the hysteresis on the desorption isotherm as shown in Figure 5 is the hydrophobicity of the surfaces of the silica gel based MCM-41. Related discussions about the hydrophobicity of the surfaces of silica gels can be found, e.g., in [9, 23, 54]. The hydrophobic surfaces of the MCM-41 is confirmed by checking the specific surface area calculated using the standard BET equation from the absorption isotherm and that from the BJH calculation, which results in that the calculated BET specific surface area is much smaller compared with that from the BJH calculation (either using the absorption or the desorption isotherm). The results of the BET specific surface area and BJH surface area of the MCM-41 sample in this study are shown in Table 4. During adsorption, the hydrophobic property of the MCM-41 surfaces makes water molecules difficult to adsorb to the hydrophobic sites at low RHs. Hence, a considerable high RH is needed to trigger the water adsorption on these sites [9, 23, 55]. While during desorption, it can be assumed that all the capillary condensed water is almost desorbed when the RH decreases to about 0.4. The reason which motivates this statement is that the porosity calculation is terminated at RH about 0.4 as discussed before, indicating that the volume of all the pores has been calculated. Hence, the moisture content measured at the RH of about 0.4 is attributed to the adsorbed water on the material surfaces. Since some sites of the MCM-41 surfaces are hydrophobic, further decreasing the RH below 0.4, the water molecules attached on these hydrophobic sites of the MCM-41 at high RHs are not stable and tend to leave the surfaces as the RH decreases. After the water on the hydrophobic sites leaves, the absorption and desorption isotherms converge at the RH around 0.3.

It can be found from Table 4 that the BJH surface area calculated from the desorption is often larger than that from the absorption (about 200 m^2/g in this case). It is because the PSD calculated

from the desorption tends to overestimate the volume of small pores since desorption only measures the pore entry or neck sizes, leading to a higher surface area compared with that calculated from the absorption. As expected, the BJH surface area calculated using the Kelvin-0 $t-$curve either from absorption or desorption is much higher compared with that using other $t-$curves. The most frequent pore radii R_{max} calculated from the absorption is larger than that from the desorption by about 0.6-0.7 nm for the different $t-$curves considered.

The differential and accumulated PSD curves calculated from the desorption isotherm for the paste CEM I are shown in Figure 16. Similar to the sample MCM-41, the PSD curves calculated from the six different $t-$curves (except that from the Kelvin-0 $t-$curve) are in relatively good agreement with each other, showing one major peak around the pore radii of 1.4 nm and two relatively small shoulders around 1.8 nm and 3.0 nm. There are also three peaks in the pore size distribution calculated using the Kelvin-0 $t-$curve, the corresponding pore radii are 1.0 nm, 1.4 nm and 2.5 nm, which are smaller compared with that using other $t-$curves. The underestimation of the pore sizes and the overestimation of the volume of small pores using the Kelvin-0 $t-$curve are more obvious in the calculated accumulate PSD curves, as shown in Figure 16b.

The differential and accumulated PSD curves calculated from the absorption isotherm for the sample CEM I are shown in Figure 17. It turns out that the different $t-$curves used affect the PSD curves calculated from the absorption isotherm in a relatively more pronounced manner compared with that calculated from the desorption isotherm, especially at the very small pore sizes. However, the two shoulders found in the pore size distribution curves using the six different $t-$curves (except that from the Kelvin-0 $t-$curve) from the desorption isotherm corresponding to the pore radii of 1.8 nm and 3 nm are also observed in the curves calculated from the absorption. The magnitude of the peak around the pore radii of 3.0 nm is comparable with the PSD curves calculated from the desorption and the absorption. A more direct comparison about the difference between the PSD curves calculated from the desorption and the absorption isotherm is shown in Figure 18. The major difference between the PSD curves calculated from the desorption and the absorption is that the most pronounced peak found from that using the desorption isotherm with the pore radii corresponding to about 1.4 nm is not found in the PSD curves calculated from the absorption. Even though it seems that there does exist one peak (or even more than one) in the calculated PSD curves using the absorption isotherm below the pore radii of 1 nm, especially in the curves using the Kelvin-0 and Halsey $t-$curves. Of this reason, it is reasonable to assume that the peak(s) may be related to the uncertainties arising from the different thickness assumed for the adsorbed layer, which might not represent the true pore size information.

The differential and accumulated PSD curves calculated from the desorption and absorption isotherm for the sample CEM III are shown from Figure 19 and Figure 20, respectively. In Figure 21, a direct comparison of the PSD curves calculated from the desorption and the absorption isotherm is shown. Similar results with respect to the peaks and the comparison between the calculated PSD curves from the absorption and desorption as found for the sample CEM I are also observed for the sample CEM III. A more direct comparison about the difference between the pore size distribution of CEM I and CEM III can be found in Figure 22a (calculated from the desorption isotherm) and Figure 22b (calculated from the absorption isotherm). It can be found that the pore radii of the peaks correspond very well in the sample CEM I and CEM III, but there are much more small pores observed in the sample CEM III, especially those pores with radii less than about 5 nm. This results are in agreement with the findings in literature, that is, the pore structure generally becomes finer with the introduction of supplementary cementitious materials, e.g. see [56–58].

The missing peak around 1.4 nm in the PSD curves calculated from the absorption isotherm compared with that calculated from the desorption isotherm deserves further discussions. Since 1.4

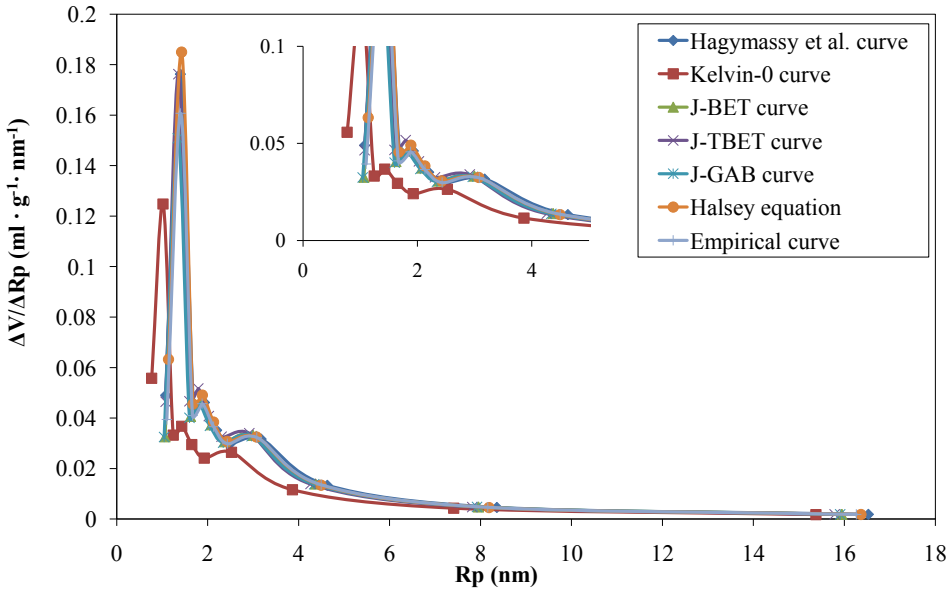

(a)

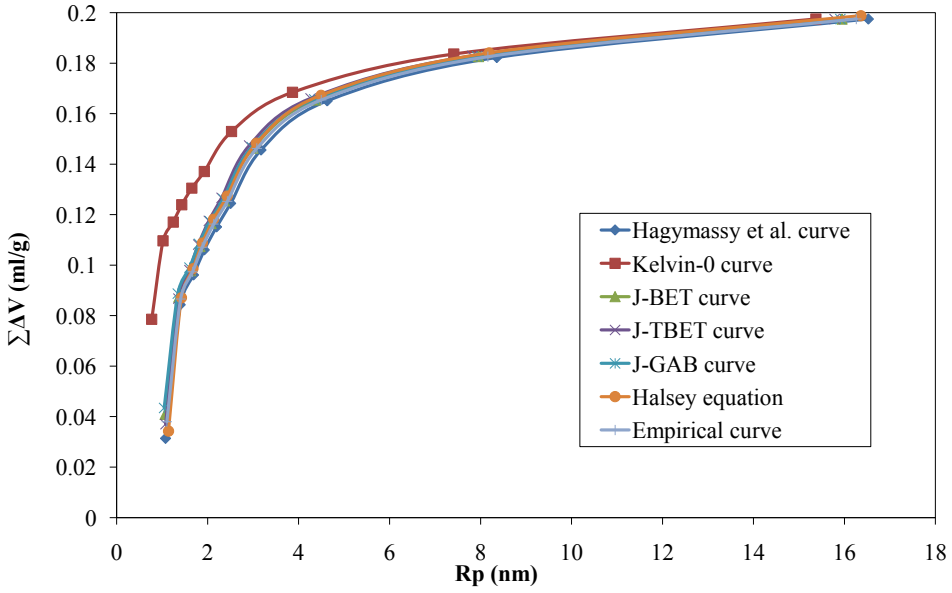

(b)

Figure 16: Pore size distribution curves of the paste CEM I calculated from the desorption isotherm using different $t-$curves: (a) differential PSD; (b) accumulated PSD.

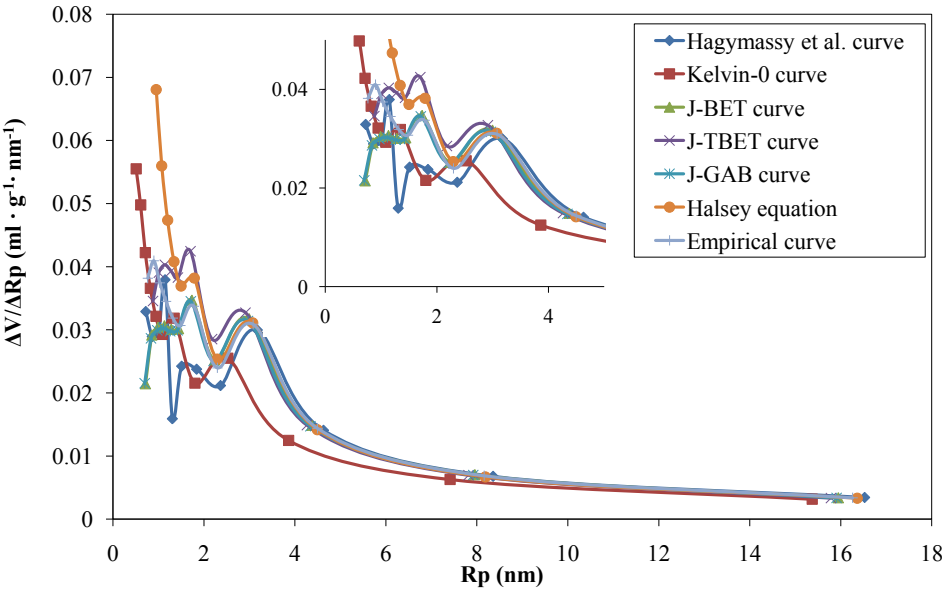

(a)

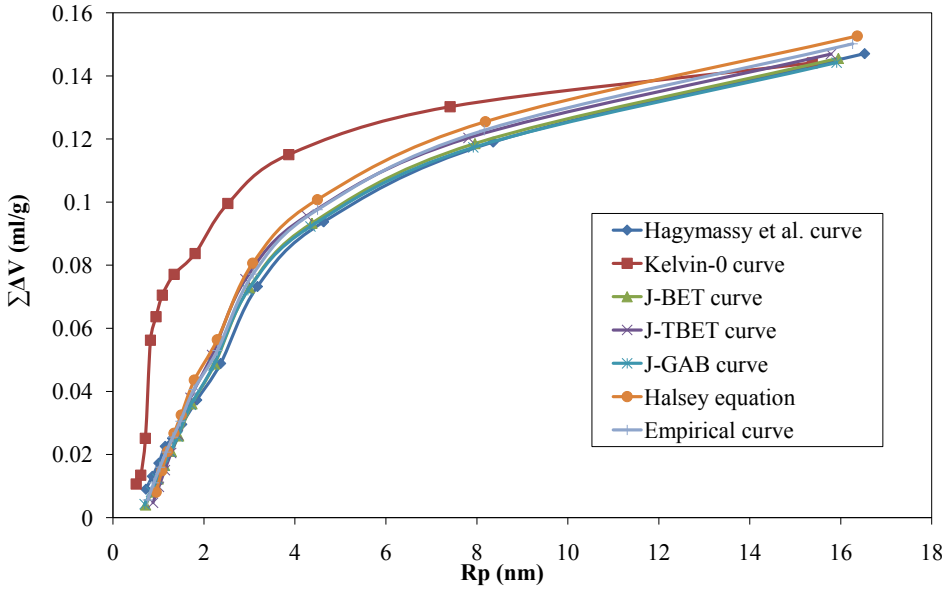

(b)

Figure 17: Pore size distribution curves of the paste CEM I calculated from the absorption isotherm using different $t-$curves: (a) differential PSD; (b) accumulated PSD.

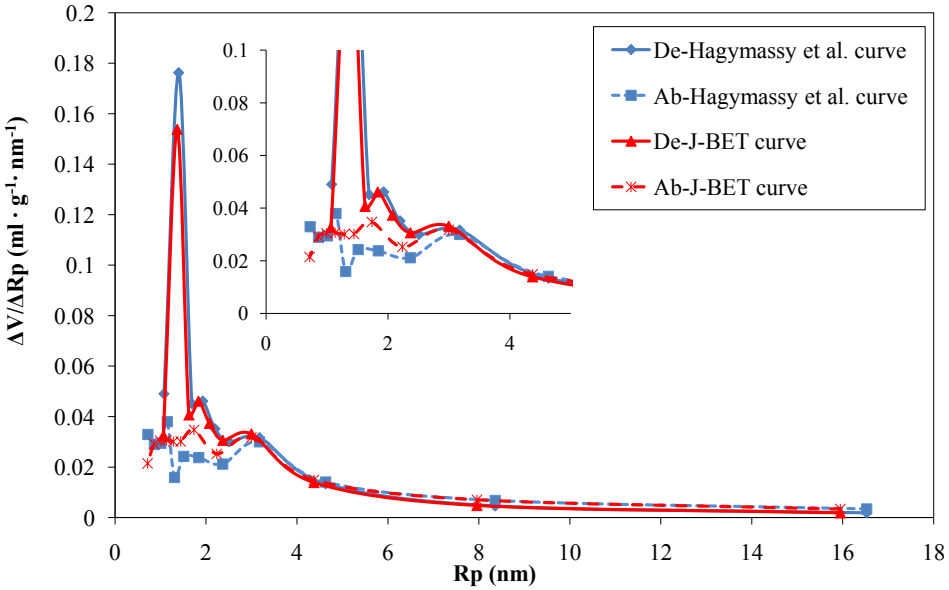

Figure 18: Comparison of the differential pore size distribution of the paste CEM I calculated from the desorption and absorption isotherms using Hagymassy et al. and J-BET $t-$curves.

nm corresponds to the RH about 0.4, one may argue the pore size peak at 1.4 nm may be related to microstructure changes (or pore structure collapse) caused by the drying effect when the RH is at this low level as discussed, e.g. in Jennings et al. [59–61], reflected by a relatively large change of the moisture content in the measured desorption isotherms. Therefore, the peak at 1.4 nm on the PSD curves calculated from the desorption isotherm should only reflect the collapse of the pore structure and should not be relevant in terms of the true pore size information. To check the relevance of the argument regarding the pore structure collapse of the studied cement pastes, a resaturation study was conducted [43]. The resaturation study went as follows: firstly a desorption-absorption cycle was applied, where the RH went down to 0 during the desorption. After that, each tested paste sample was resaturated with distilled water. Following that, a second desorption-absorption cycle was applied on the resaturated samples. The sorption isotherms (both desorption and absorption) of the resaturated samples were concluded to be identical to what was measured during the first desorption-absorption cycle. That is to say, if the microstructure changes caused by the so-called drying at low RHs take place, the resaturation of the sample after a desorption measurement must be able to fully restore the pore structure. However, if the microstructure changes are assumed relevant in this context, it seems difficult to understand when and how the restoration of the pore structure takes place in the absorption. Obviously the restoration does not take place around the RH of 0.4 (as the peak around this RH is missing in absorption curves), but it will be restored anyway (as discussed in the resaturation study). Thus, it turns out to be difficult to find convincing evidence to attribute the peak around 1.4 nm purely to the microstructure changes which might occur during the desorption. However, if the network effect is taken into consideration, the peak around 1.4 nm observed on the PSD curves calculated from the desorption isotherm can be better explained. According to the concept of the network effect, one can assume that this 1.4 nm should correspond to the radii of pore entries or necks which are probably connected to many pores with bigger interior sizes. During desorption, water in

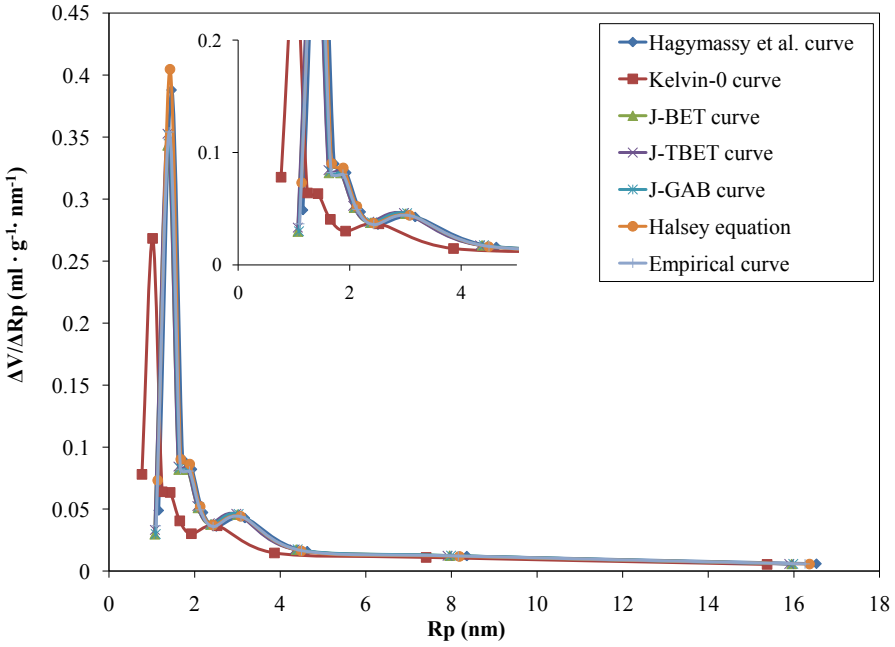

(a)

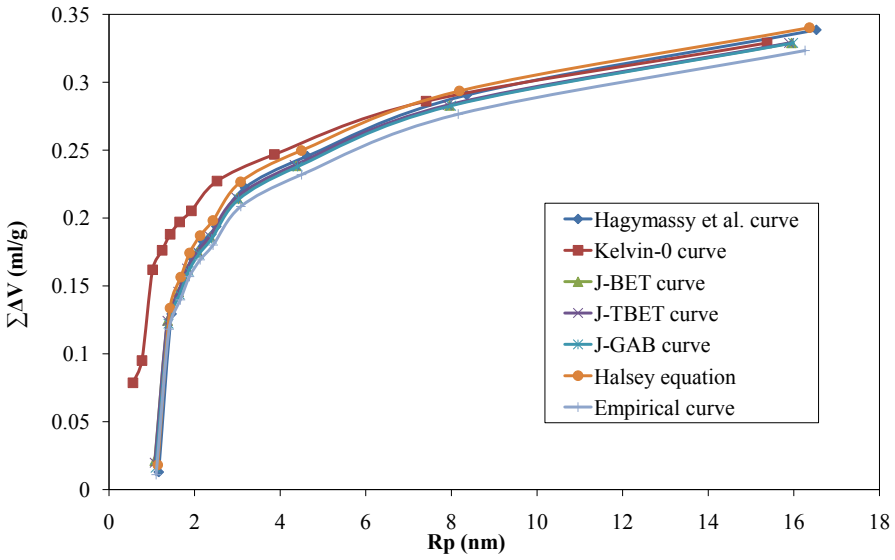

(b)

Figure 19: Pore size distribution curves of the paste CEM III calculated from the desorption isotherm using different $t-$curves: (a) differential PSD; (b) accumulated PSD.

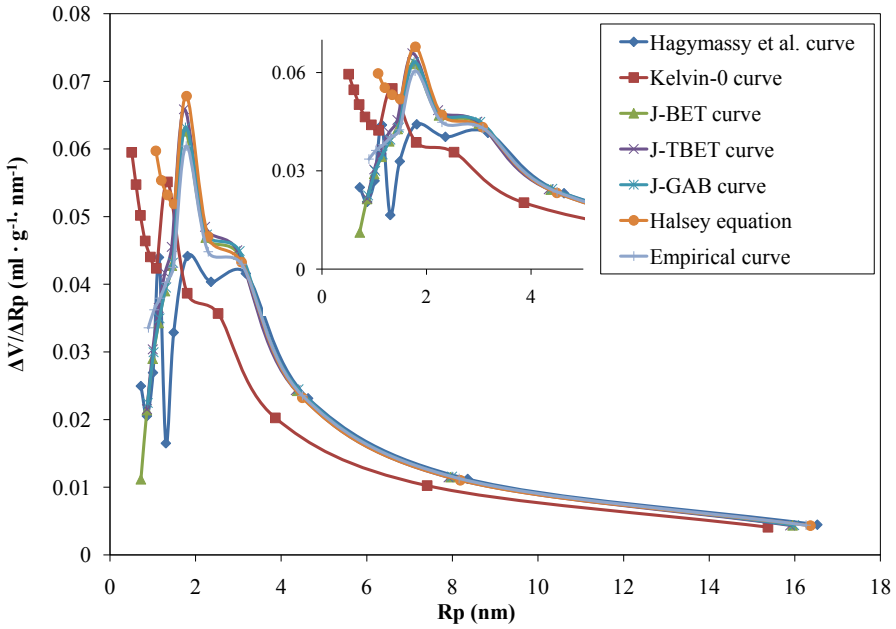

(a)

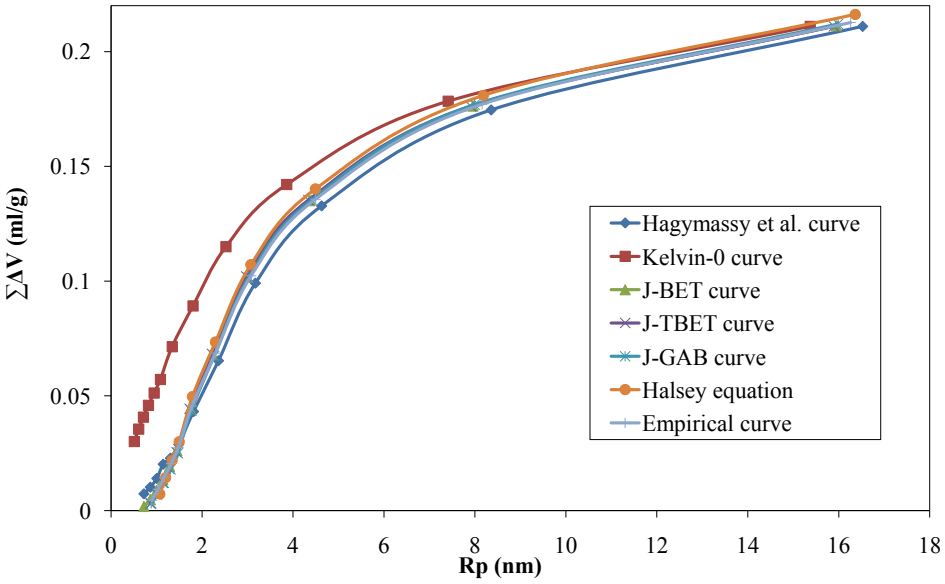

(b)

Figure 20: Pore size distribution curves of the paste CEM III calculated from the absorption isotherm using different $t-$curves: (a) differential PSD; (b) accumulated PSD.

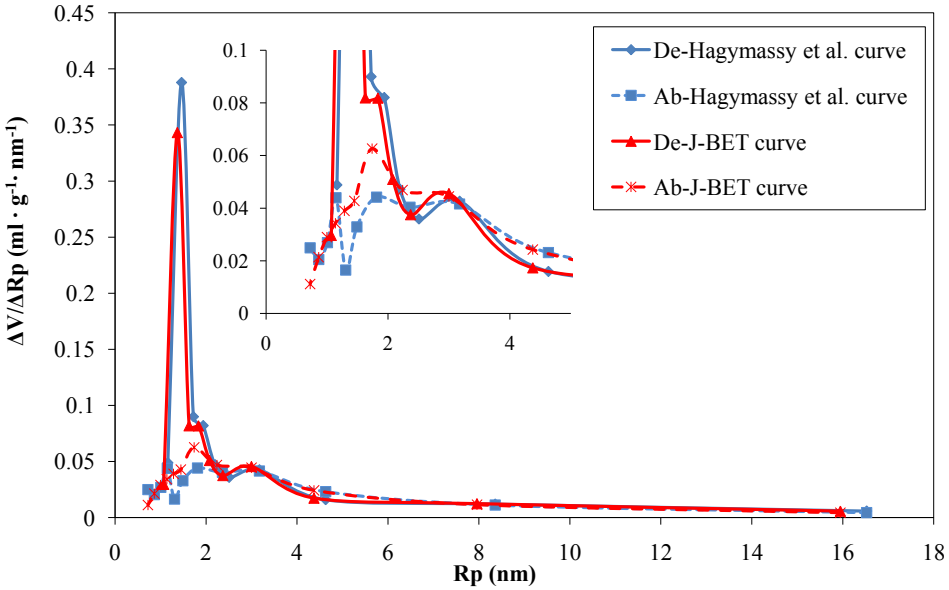

Figure 21: Comparison of the differential pore size distribution of the paste CEM III calculated from the desorption and absorption isotherms using Hagymassy et al. and J-BET $t-$curves.

these bigger pores can only be emptied when the water in the entries and necks has been desorbed. This effect might be the reason for why the calculated relatively big peak around 1.4 nm is observed on desorption curves. While during absorption, the pores are gradually filled at the RHs corresponding to their interior sizes as determined by the Kelvin equation. The implication of the comparison between the PSD results calculated from the desorption and the absorption isotherm to a large extent can be understood as that 1.4 nm is an important size of the pore entries or necks to which big pores are connected in the cement paste samples.

The BET specific surface area and the surface area calculated from the BJH method for the pastes CEM I and CEM III are listed in Table 5. Similar to what has been found for the MCM-41, the BJH surface area calculated from the desorption isotherm is much bigger than that from the absorption isotherm. It is also noticed that the calculated BJH surface area from absorption fits very well with the BET specific surface area, except that using the Kelvin-0 $t-$curve. The relatively higher BJH surface area using the Kelvin-0 $t-$curve can be attributed to the overestimation of the small pores as discussed before. With respect to the difference between the BJH surface area calculated from the desorption and absorption isotherm, a reasonable explanation can be formulated by taking into account the network theory, which is that the desorption measurement only reflects the pore entry or neck sizes rather than the interior sizes of the pores. Following this concept, it can be imagined that the calculation using the desorption data actually overestimates the volume of small pores, resulting into a higher surface area compared with the BET value, which is in accordance with what is shown in Table 5. The agreement between the BJH surface area calculated from the absorption and the BET specific surface area in this study might indicate that it is actually more reasonable to use the absorption isotherm to calculate the pore size distribution, as recommended in [8, 31, 38, 39]. On the other hand, since the desorption isotherm also can provide information about the network effect, a combined study of both the desorption and the absorption isotherms may give a more detailed picture

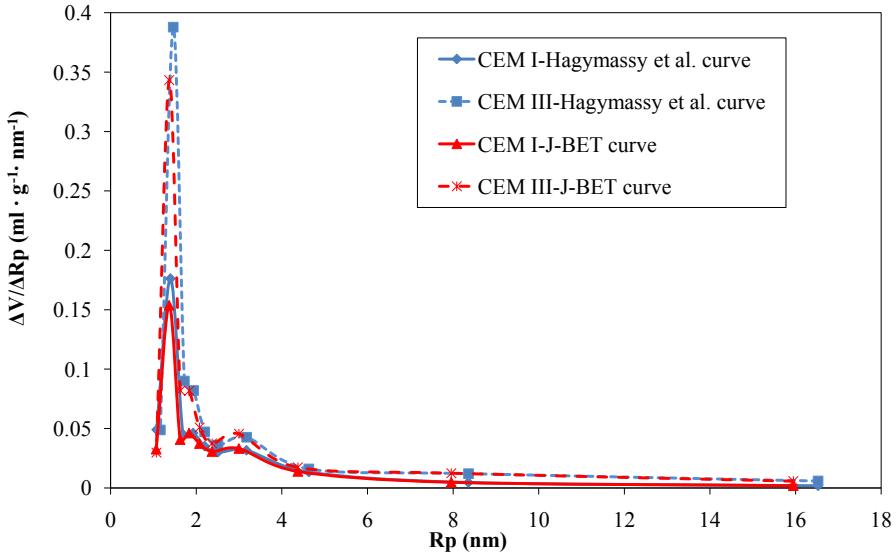

(a)

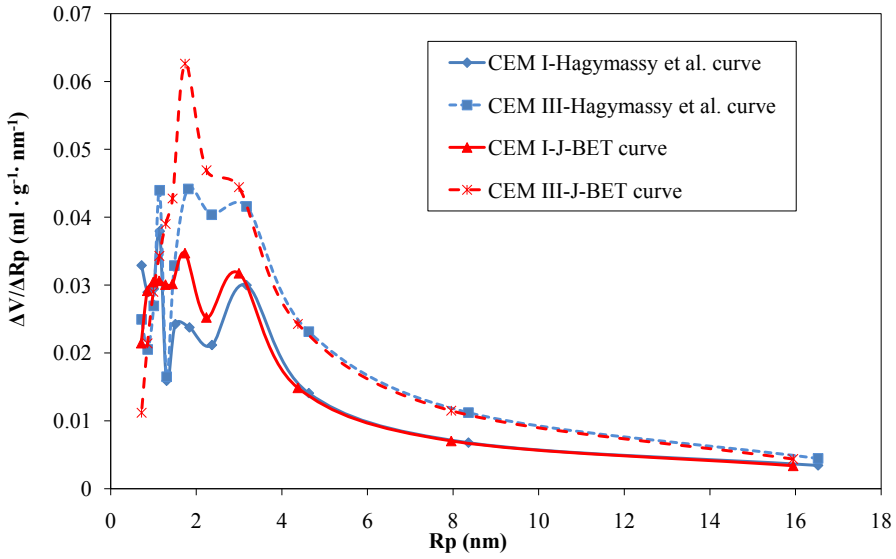

(b)

Figure 22: Comparison of the differential pore size distribution curves of the pastes CEM I and CEM III calculated from (a) the desorption isotherm and (b) the absorption isotherm using Hagymassy et al. and J-BET $t-$curves.

Table 5: The calculated BJH surface area and the BET specific surface area (m^2/g) for the two hardened cement pastes CEM I and CEM III.

Items		CEM I		CEM III	
		absorption	desorption	absorption	desorption
BJH	Hagymassy et al. curve	119	196	146	294
	Kelvin-0 curve	164	204	183	331
	J-BET curve	111	169	138	281
	J-TBET curve	110	185	141	286
	J-GAB curve	112	169	139	282
	Halsey equation	116	214	143	308
	Empirical curve	117	181	140	285
BET		112		135	

about the porosity characteristics of the material under study.

4. Conclusions

Sorption behavior of water vapor on a porous material can be used to study important characteristics of the material, e.g., the specific surface area and the pore size distribution. In this work, the specific surface area was calculated based on different equations accounting for multilayer adsorption and the pore size distribution was derived from both the absorption and the desorption isotherms using different $t-$curves for two hardened cement pastes (CEM I and CEM III) and one model porous material (MCM-41). Some important points of this investigation can be summarized as follows.

1. The calculated specific surface area is very much dependent on the equations considered for multilayer adsorption. For the studied materials, the specific surface area calculated based on the two-layer BET equation was smaller than that based on the standard BET equation. The relative difference for sample MCM-41 and CEM I wass about 26% and 24%, respectively; while the relative difference was much smaller for the paste CEM III (less than 1%). The specific surface area calculated from the GAB equation was bigger than that obtained by the standard BET equation for sample MCM-41 and sample CEM I while the opposite relation was found for the paste CEM III. These somewhat inconsistent results were suspected to be due to the fitted GAB parameter k. The best fitted k value for both the MCM-41 and the CEM I were less than 1 while the value obtained for CEM III was larger than 1.
2. Various $t-$curves were assumed accounting for the thickness of the adsorbed layer in calculating the pore size distribution. Except the Kelvin-0 $t-$curve, which assumes 0 thickness for the adsorbed layer, the pore size distribution calculated from either the desorption or the absorption isotherm shows reasonable agreement. For the model material MCM-41, the most frequent pore radii R_{max} found using the desorption isotherm is in the range of 1.7 nm to 1.9 nm compared with 2.4 nm to 2.6 nm when using the absorption counterpart. For the hardened cement pastes CEM I and CEM III, three characteristic peaks are found in the PSD curves calculated from the desorption isotherm with corresponding radii of 1.4 nm, 1.8 nm and 3.0 nm while the peak at 1.4 nm is missing and only two peaks are found in the PSD curves calculated using the absorption isotherm. This may indicate that 1.4 nm is an important size of the pore entries or necks to which bigger pores are connected in the investigated cement paste samples.
3. For the model material MCM-41, the calculated BJH surface area (using either the absorption or the desorption isotherm) was much bigger than the calculated BET specific surface area.

The reason for this could probably be related to the hydrophobic properties of its surface. Additionally, the BJH surface area calculated from the desorption isotherm was also bigger than that calculated from the absorption isotherm, which could be explained by that fact that the calculation using the desorption isotherm overestimates the volume of small pores, leading to a relatively high calculated surface area. The same conclusion holds for the hardened cement pastes in terms of the difference observed between the BJH surface area calculated using the desorption and the absorption isotherms. However, since the surface of hardened cement paste samples is hydrophilic, the BJH surface area, especially that calculated from the absorption isotherm, was much closer to the BET specific surface area for the two studied hardened cement pastes.

4. The network theory, which states that the desorption is controlled by the pore entry or neck sizes while the absorption is controlled by the real pore sizes, tends to be of great relevance in explaining some of the results, including the hysteresis behavior, the difference between the calculated pore size distribution curves and the difference in the BJH surface areas calculated from the desorption and the absorption isotherms.

Acknowledgment

The research leading to these results has received funding from the European Union Seventh Framework Programme (FP7/2007-2013) under grant agreement 264448.

References

[1] T. Allen. *Particle size measurement: Powder sampling and particle size measurement*, volume 2. Springer, 5th edition, 1997.

[2] K. Sing, D. Everett, R. Haul, L. Moscou, R. Pierotti, J. Rouquerol, and T. Siemieniewska. Reporting physisorption data for gas/solid systems. *Pure Appl. Chem*, 57(4):603–619, 1985.

[3] S. Brunauer, P.H. Emmett, and E. Teller. Adsorption of gases in multimolecular layers. *Journal of the American Chemical Society*, 60(2):309–319, 1938.

[4] E.P. Barrett, L.G. Joyner, and P.P. Halenda. The determination of pore volume and area distributions in porous substances. I. computations from nitrogen isotherms. *Journal of the American Chemical Society*, 73(1):373–380, 1951.

[5] M. Janz and B.F. Johannesson. Measurement of the moisture storage capacity using sorption balance and pressure extractors. *Journal of Building Physics*, 24(4):316–334, 2001.

[6] V. Kocherbitov and L. Wadsö. A desorption calorimetric method for use at high water activities. *Thermochimica Acta*, 411(1):31–36, 2004.

[7] K. S. W. Sing. *Colloid Science*, volume 1. Royal Society of Chemistry, 1973. doi: 10.1039/9781847557421-00001.

[8] K. Sing. The use of nitrogen adsorption for the characterisation of porous materials. *Colloids and Surfaces A: Physicochemical and Engineering Aspects*, 187:3–9, 2001.

[9] J. Hagymassy, S. Brunauer, and R.S. Mikhail. Pore structure analysis by water vapor adsorption: I. t-curves for water vapor. *Journal of Colloid and Interface Science*, 29(3):485–491, 1969.

[10] J. Villadsen. Pore structure in cement based materials. Technical Report 277, Building Materials Laboratory, Technical University, Denmark, 1992.

[11] I. Langmuir. The constitution and fundamental properties of solids and liquids. Part I. solids. *Journal of the American Chemical Society*, 38(11):2221–2295, 1916.

[12] B. Johannesson. Moisture fixation in mature concrete and other porous materials (8A). Lecture notes for Introduction to Concrete Technology (11563), Technical University of Denmark, 2011.

[13] B. Johannesson. *Transport and sorption phenomena in concrete and other porous media.* PhD thesis, Division of Building Materials, Lund University, 2000.

[14] I. Wadsö and L. Wadsö. A new method for determination of vapour sorption isotherms using a twin double microcalorimeter. *Thermochimica Acta*, 271:179–187, 1996.

[15] L. Wadsö and N. Markova. A double twin isothermal microcalorimeter. *Thermochimica Acta*, 360(2):101–107, 2000.

[16] E.A. Guggenheim. Application of statistical mechanics. Clarendon, 1966.

[17] R.B. Anderson. Modifications of the Brunauer, Emmett and Teller equation1. *Journal of the American Chemical Society*, 68(4):686–691, 1946.

[18] J.H. De Boer, editor. *The dynamical character of adsorption.* Clarendon Press, Oxford, UK, 2nd edition, 1968.

[19] C. Van den Berg. *Vapour sorption equilibria and other water-starch interactions: a physico-chemical approach.* PhD thesis, Wageningen Agricultural University, the Netherlands, 1981.

[20] R. W. Dent. A multilayer theory for gas sorption. Part I: Sorption of a single gas. *Textile Research Journal*, 47(2):145–152, 1977.

[21] R.W. Dent. A sorption theory for gas mixtures. *Polymer Engineering & Science*, 20(4):286–289, 1980.

[22] S. Brunauer, J. Skalny, and E.E. Bodor. Adsorption on nonporous solids. *Journal of Colloid and Interface Science*, 30(4):546–552, 1969.

[23] A. Raoof, J.P. Guilbaud, H. Van Damme, P. Porion, and P. Levitz. Analysis of the multilayer thickness relationship for water vapor and nitrogen adsorption. *Journal of Colloid and Interface Science*, 206(1):1–9, 1998.

[24] V. Baroghel-Bouny. Water vapour sorption experiments on hardened cementitious materials: Part I: Essential tool for analysis of hygral behaviour and its relation to pore structure. *Cement and Concrete Research*, 37(3):414–437, 2007.

[25] R.M. Espinosa and L. Franke. Inkbottle pore-method: Prediction of hygroscopic water content in hardened cement paste at variable climatic conditions. *Cement and Concrete Research*, 36(10): 1954–1968, 2006.

[26] O. Šolcová, L. Matějová, and P. Schneider. Pore-size distributions from nitrogen adsorption revisited: Models comparison with controlled-pore glasses. *Applied Catalysis A: General*, 313(2): 167–176, 2006.

[27] C.G. Shull, P.B. Elkin, and L.C. Roess. Physical studies of gel microstructure. *Journal of the American Chemical Society*, 70(4):1410–1414, 1948.

[28] A. Wheeler. Reaction rates and selectivity in catalyst pores. In P.H. Emmett, editor, *Catalysis Part II.*, page 105. Rheinhold Publ. Corp., 1955.

[29] D.H. Everett and W.I. Whitton. A general approach to hysteresis. *Transactions of the Faraday Society*, 48:749–757, 1952.

[30] J.H. De Boer. *The Structure and properties of porous materials*. Proceedings of the Symposium of the Colston Research Society. Butterworths, 1958.

[31] K.S.W. Sing. Characterization of porous materials: past, present and future. *Colloids and Surfaces A: Physicochemical and Engineering Aspects*, 241(1):3–7, 2004.

[32] Z.P. Bažant and M.Z. Bazant. Theory of sorption hysteresis in nanoporous solids: Part I snap-through instabilities. *Journal of the Mechanics and Physics of Solids*, 60(9):1644–1659, 2012.

[33] M.Z. Bazant and Z.P. Bažant. Theory of sorption hysteresis in nanoporous solids: Part II molecular condensation. *Journal of the Mechanics and Physics of Solids*, 60(9):1660–1675, 2012.

[34] P.J. Branton, P.G. Hall, K.S.W. Sing, H. Reichert, F. Schüth, and K.K. Unger. Physisorption of argon, nitrogen and oxygen by MCM-41, a model mesoporous adsorbent. *J. Chem. Soc., Faraday Trans.*, 90(19):2965–2967, 1994.

[35] P.I. Ravikovitch, S.C.Ó. Domhnaill, A.V. Neimark, F. Schüth, and K.K. Unger. Capillary hysteresis in nanopores: theoretical and experimental studies of nitrogen adsorption on MCM-41. *Langmuir*, 11(12):4765–4772, 1995.

[36] P.J. Branton, P.G. Hall, and K.S.W. Sing. Physisorption of alcohols and water vapour by MCM-41, a model mesoporous adsorbent. *Adsorption*, 1(1):77–82, 1995.

[37] P.J. Branton, K.S.W. Sing, and J.W. White. Adsorption of carbon tetrachloride and nitrogen by 3.4 nm pore diameter siliceous MCM-41. *J. Chem. Soc., Faraday Trans.*, 93(13):2337–2340, 1997.

[38] N.A. Seaton. Determination of the connectivity of porous solids from nitrogen sorption measurements. *Chemical Engineering Science*, 46(8):1895–1909, 1991.

[39] K.S.W. Sing. Adsorption methods for the characterization of porous materials. *Advances in Colloid and Interface science*, 76:3–11, 1998.

[40] G.C. Wall and R.J.C. Brown. The determination of pore-size distributions from sorption isotherms and mercury penetration in interconnected pores: The application of percolation theory. *Journal of Colloid and Interface Science*, 82(1):141–149, 1981.

[41] V.P. Zhdanov, V.B. Fenelonov, and D.K. Efremov. Determination of pore-size distribution from sorption isotherms: Application of percolation theory. *Journal of Colloid and Interface Science*, 120(1):218–223, 1987.

[42] E.L. Perkins, J.P. Lowe, K.J. Edler, N. Tanko, and S.P. Rigby. Determination of the percolation properties and pore connectivity for mesoporous solids using NMR cryodiffusometry. *Chemical Engineering Science*, 63(7):1929–1940, 2008.

[43] M. Wu, B. Johannesson, and M. Geiker. A study of the water vapor sorption isotherms of hardened cement pastes: possible pore structure changes at low relative humidity and the impact of temperature on isotherms. *Cement and Concrete Research*, 56:97–105, 2014.

[44] B. Johannesson and P. Utgenannt. Microstructural changes caused by carbonation of cement mortar. *Cement and Concrete Research*, 31(6):925–931, 2001.

[45] V.T. Ngala and C.L. Page. Effects of carbonation on pore structure and diffusional properties of hydrated cement pastes. *Cement and Concrete Research*, 27(7):995–1007, 1997.

[46] J.J. Thomas, H.M. Jennings, and A.J. Allen. The surface area of hardened cement paste as measured by various techniques. *Concr. Sci. Eng*, 1:45–64, 1999.

[47] H.H. Willems and K.B. Van Der Velden. A gravimetric study of water vapour sorption on hydrated cement pastes. *Thermochimica Acta*, 82(1):211–220, 1984.

[48] M. Åhs. *Redistribution of moisture and ions in cement based materials.* PhD thesis, Division of Building Materials, Lund University, 2011.

[49] E.O. Timmermann. Multilayer sorption parameters: BET or GAB values? *Colloids and Surfaces A: Physicochemical and Engineering Aspects*, 220(1-3):235–260, 2003.

[50] T. Sneck, L. Kinnunen, and H. Oinonen. *Measurements of Pore Size Distribution of Porous Materials: Interim Report.* State Institute for Technical Research, Helsinki, Finland, 1966.

[51] C.M. Lastoskie and K.E. Gubbins. Characterization of porous materials using density functional theory and molecular simulation. *Studies in Surface Science and Catalysis*, 128:41–50, 2000.

[52] P.I. Ravikovitch and A.V. Neimark. Characterization of nanoporous materials from adsorption and desorption isotherms. *Colloids and Surfaces A: Physicochemical and Engineering Aspects*, 187:11–21, 2001.

[53] S.J. Gregg and K.S.W. Sing. *Adsorption, surface area, and porosity.* Academic Press, London, 2 edition, 1982.

[54] F.A. Shebl, M. Abd El-Khalik, and F.M. Helmy. Theoretical studies on the standard but misleading adsorption isotherm I: True adsorption isotherm. *Surface technology*, 19(4):321–334, 1983.

[55] V. Kocherbitov and V. Alfredsson. Hydration of MCM-41 studied by sorption calorimetry. *The Journal of Physical Chemistry C*, 111(35):12906–12913, 2007.

[56] R.D. Hooton. Permeability and pore structure of cement pastes containing fly ash, slag, and silica fume. *Blended Cements, ASTM STP*, 897:128–143, 1986.

[57] V.M. Malhotra. *Supplementary cementing materials for concrete.* Special publication / Canada Centre for Mineral and Energy Technology ; SP86-8E. Energy, Mines, and Resources Canada, Canada Centre for Mineral and Energy Technology, 1987.

[58] A.M. Neville. *Properties of concrete.* Prentice Hall, 4th edition edition, 1995.

[59] H.M. Jennings. A model for the microstructure of calcium silicate hydrate in cement paste. *Cement and Concrete Research*, 30(1):101–116, 2000.

[60] J.J. Thomas and H.M. Jennings. A colloidal interpretation of chemical aging of the C-S-H gel and its effects on the properties of cement paste. *Cement and Concrete Research*, 36(1):30–38, 2006.

[61] H.M. Jennings. Refinements to colloid model of C–S–H in cement: CM–II. *Cement and Concrete Research*, 38(3):275–289, 2008.